

# POLITECNICO DI TORINO

Master's Degree in Aerospace Engineering



Master's Degree Thesis

## Analysis of parking orbits for round-trip Mars missions

Supervisors

Prof. Lorenzo CASALINO

Candidate

Alice NERVO

December 2020

## Abstract

A round-trip mission to Mars, whether manned or unmanned, presents a great number of engineering challenges in all fields of the mission architecture. In particular, the human exploration of Mars is widely considered to be the next great frontier for space engineering. The hurdles of this type of mission vary largely, from space medicine to the project of a vehicle able to leave the Mars surface. The choice of the parking orbits around Mars, which is the subject of this thesis, is fundamental too, as it needs to ensure Mars capture and escape of the spacecraft, with the minimal expense of propellant. This translates into a necessary optimization of the total DV.

In the context of this master thesis, the bi-elliptic apotwist method of parking orbits selection, developed by Qu, Merrill, Chai and Komar, is presented and analyzed. This technique consists of seven burns, including three "apotwists", namely plane change maneuvers performed at apoapsis. The bi-elliptic apotwist method performs better in terms of total DV compared to more traditional 2-burns sequence. Furthermore, it has been developed a MATLAB code that computes the optimization of the total DV of the seven maneuvers using a genetic algorithm, which theory is also presented in one of the chapters. The code's results have been obtained using pre-existing data to verify its quality and a mass estimation has been proposed.



# Acknowledgements

In conclusion of my master degree studies, I need to thank the people that helped me during the past years and, in particular, in writing this thesis.

Firstly, I would like to thank my supervisor, Professor Lorenzo Casalino, for his time, guidance and assistance throughout the development of this thesis study.

I also would like to thank my family and friends, for always offering a word of comfort and a hand of help during my lowest moments. I could not have done it without you all.



# Table of Contents

<b>List of Tables</b>	VI
<b>List of Figures</b>	VII
<b>1 Round-trip missions to Mars</b>	<b>1</b>
1.1 Introduction . . . . .	1
1.2 Human Round-trip Mission Architecture . . . . .	2
1.3 Optimization of Mars parking orbits . . . . .	3
<b>2 Genetic algorithms</b>	<b>6</b>
2.1 History of evolutionary and genetic algorithms . . . . .	6
2.2 Terminology . . . . .	7
2.3 Genetic algorithm structure and characteristics . . . . .	8
2.4 Creation of the initial population . . . . .	9
2.5 Fitness computation . . . . .	10
2.6 Parents selection . . . . .	11
2.6.1 Proportionate selection . . . . .	12
2.6.2 Rank selection . . . . .	13
2.6.3 Tournament selection . . . . .	14
2.7 Reproduction . . . . .	14
2.7.1 Crossover . . . . .	14
2.7.2 Mutation . . . . .	15
2.8 Termination . . . . .	18
2.9 Genetic algorithms in MATLAB . . . . .	18
<b>3 Physical model</b>	<b>21</b>
3.1 Laws controlling orbital mechanics . . . . .	21
3.2 The two-body problem . . . . .	22
3.2.1 Constants of motion . . . . .	23
3.3 Trajectory Equation . . . . .	24
3.4 Conic sections geometry . . . . .	25

3.4.1	Relating orbit geometry and constants of motion . . . . .	27
3.4.2	Elliptical orbits . . . . .	28
3.4.3	Hyperbolic orbits . . . . .	28
3.5	Coordinate systems . . . . .	29
3.5.1	The Equatorial Coordinate System . . . . .	29
3.5.2	The Right Ascension-Declination System . . . . .	30
3.5.3	The Perifocal Coordinate System . . . . .	31
3.6	Classical orbital elements . . . . .	31
3.6.1	Determination of the orbital elements from position and velocity vectors . . . . .	32
<b>4</b>	<b>Optimization study</b>	<b>35</b>
4.1	The bi-elliptic apotwist technique . . . . .	35
4.2	Methodology . . . . .	37
4.3	Analytical Development . . . . .	38
4.3.1	Capture and Escape . . . . .	39
4.3.2	Plane change at apoapsis . . . . .	44
4.3.3	Apoapsis height variation . . . . .	45
4.3.4	Perturbations propagation . . . . .	45
4.4	MATLAB implementation . . . . .	46
4.5	Results . . . . .	47
4.5.1	Orbital missions comparison . . . . .	48
4.5.2	The 2041 mission analysis . . . . .	51
<b>5</b>	<b>Conclusions</b>	<b>56</b>
	<b>Bibliography</b>	<b>58</b>

# List of Tables

2.1	Initial population example . . . . .	10
2.2	List of MATLAB GA elements . . . . .	19
2.3	List of possible user options for MATLAB GA . . . . .	20
4.1	Summary of the seven burns of the bi-elliptic apotwist . . . . .	36
4.2	Optimization algorithm input parameters . . . . .	38
4.3	Optimization variables . . . . .	38
4.4	Hyperbolic trajectories data[17] . . . . .	48
4.5	$\Delta V$ of the three different missions . . . . .	49
4.6	2 burns technique comparison . . . . .	50
4.7	Influence of the variation of $a_{PO}$ on $\Delta V$ . . . . .	51
4.8	Mass data[19] . . . . .	54
4.9	Mass analysis results . . . . .	55

# List of Figures

1.1	Mission sequence summary [5]	4
2.1	Genetic algorithm scheme	9
2.2	Proportionate selection scheme	13
2.3	Reproduction scheme	15
2.4	Different crossover methods scheme	16
2.5	Mutation scheme	16
3.1	Two-body problem	23
3.2	Flight path angle	24
3.3	Conic sections	25
3.4	Elements of a conic section [16]	26
3.5	Classical orbital elements [16]	32
4.1	Bi-elliptic apotwist representation [6]	37
4.2	MCPS design [19]	54



# Chapter 1

## Round-trip missions to Mars

### 1.1 Introduction

Mars is the most geologically similar planet to the Earth in the Solar System. It is also, together with Venus, the most accessible planet to a spacecraft, thanks to its relative closeness, but, contrary to Venus, Mars conditions also make it suitable for exploration. This has certainly awakened a peculiar scientific and social interest in the Red Planet, that is most likely the first planet outside Earth where humans will set foot in the future [1].

Studies over the past decades also confirmed the presence of water on Mars, concentrated on its poles in form of ice and present in small amounts in the atmosphere in form of vapor [2]. Furthermore, evidences of flowing water on the planet's surface have already been found, such as the apparent existence of shorelines and rivers [3]. This has lead many to believe the possibility of past or present life on its surface, though this is still only a plausible hypothesis. In fact, water, and especially liquid water, is necessary to life as we understand it today.

In present conditions, there is no liquid water on Mars surface, and also it cannot exist in liquid state. This is due to the fact that the planet's pressure, which is approximately of 0.007 bar, is so low that water changes state directly from solid to vapor. Salts dissolved in water, though, lower the freezing point, possibly allowing liquid water to exist.

Therefore, currently, the main scientific purposes to further explore Mars are [4]:

- Search for life.
- Study the planet's surface, atmosphere and their evolution.

- Prepare for future human exploration.

The search for life on Mars is based on one of the fundamental philosophical and biological questions of humankind, whether life exists anywhere in the Universe outside our planet. Evidences of life on Mars, which is the most accessible place to look for at the state of art of technology, would be a revolutionary discovery for science as a whole.

Mars was once a much different planet. In particular, its atmosphere varied drastically, experiencing some severe climate change. This can be studied and understood with planetary geology, to unveil the history of Mars surface, and the analysis of samples of Mars thin atmosphere. Of course, the knowledge that can be acquired studying Mars evolution, can be used to understand better the Earth and the entire Solar System.

Human exploration of the Red Planet, though, is the greatest challenge for Space Engineering and the most dangerous one. To prepare for a human mission, more robotic missions are needed, to fully understand the hazards to human life that the martian surface discloses, to reduce risks to the minimum, specifically for the first trips, and return the crew safely to Earth. Furthermore, the selection of a landing site is fundamental, as it might ensure the presence or not of water, that in this way will not need to be completely stored from Earth.

A round-trip mission to Mars could be both manned or unmanned. An unmanned mission of sample and return, other than technologically prepare for a human mission, could help understand Mars geology much better, studying samples in Earth laboratories, rather than in orbit. A round-trip mission, instead, is obviously necessary for manned mission to return the astronauts safely to Earth. Both these cases require rapid missions, especially the manned ones. In fact, the human body is not fully apt to live under space environment conditions. Space medicine is not advanced enough to fully understand the impact of space conditions on the astronauts health, but, certainly, limiting their time in such a dangerous environment is fundamental. It is therefore necessary to reduce the transfer time and the stay time on the target planet surface.

## 1.2 Human Round-trip Mission Architecture

In this section, it will be briefly presented the architecture for the first human mission to Mars, according to NASA's latest to date *Human Exploration of Mars, Design Reference Architecture 5.0* [5].

A human mission to Mars requires a very large mass to be delivered to the target planet, in order to cover all the crew necessities in flight and on the planet surface, and ensure the return to Earth. Therefore, numerous heavy-lift cargo launches

are necessary to deliver the mass to a LEO orbit. This phase has to begin several months prior to the actual Mars departure window, to have margin for delays.

Part of the surface mission elements will be pre-deployed to Mars orbit, ahead of the crew arrival. This is the first phase of this mission architecture. In particular, the Descent/Ascent Vehicle (DAV) and the surface habitat (SHAB). These two elements will be pre-deployed into a low-energy trajectory from Earth to Mars, as there is no need for a rapid transfer that would cost significantly more. The SHAB will stay in a high-Mars orbit until the arrival of the crew, while the DAV will autonomously land on Mars surface at a given landing site. This calls for the ability of these infrastructures to operate completely without human presence to allow the astronauts to have them at their disposal, as soon as they arrive on Mars.

The second phase of this architecture consists of the insertion into a fast-transit Mars transfer orbit of the crew vehicle, the Mars Transfer Vehicle (MTV), after all systems, including the pre-deployed infrastructures, have been verified as operational. The transfer time varies from different mission dates, and ranges from 175 days and 225 days. At arrival on Mars, the crew performs a rendezvous with the SHAB, which serves as the lander to Mars surface.

The crew will carry out the exploration of the surface for a stay time that would approximately be of 18 months. During this third phase, the focus will be on science and exploration activities. In particular, the main objectives of human exploration are officially summarized as:

- *Planetary Science*: scientific studies of astrobiology, climatology and geology of Mars.
- *Preparation for Sustained Human Presence*: preparation for a possible future continuous human presence on Mars and a possible colonization.
- *Ancillary Science*: scientific objectives not directly related to Mars, including astronomical observations. This objective is more important to the transfer phase from Earth to Mars and vice versa.

After a checkout of all systems involved, the last phase of this mission architecture begins, as the astronauts ascend back to orbit and then return to Earth. The surface infrastructures are left in dormant state, for a potential future use.

The entire mission architecture is summarized in figure 1.1.

### 1.3 Optimization of Mars parking orbits

After the definition of a mission architecture and its primary requirements, it is fundamental to study the trajectories that will allow the spacecraft to reach Mars and return from it, as well as those orbits where the spacecraft will be left until the

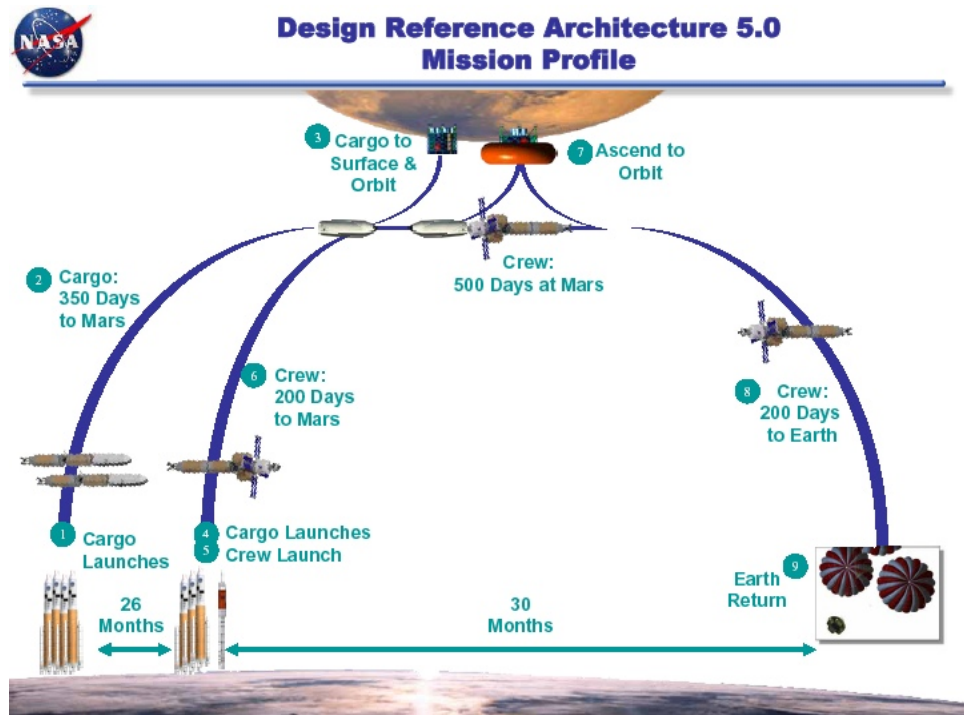


Figure 1.1: Mission sequence summary [5]

crew ascend back to orbit and departs to Earth. These orbits, which are within Mars sphere of influence, are called parking orbits. It is necessary to study the optimization of these orbits and their coupling with the interplanetary trajectories within the design process of a round-trip mission [6].

Once at arrival in Mars sphere of influence, the spacecraft must perform maneuvers to reach the desired orbit for the specific mission. In the same way, it has to reorient to find itself in a particular orbit to perform the escape sequence and return to Earth. The goal of the optimization of Mars parking orbits is to reduce the cost of these reorientation maneuvers to the minimum, in terms of total  $\Delta V$  required, which obviously translates to propellant mass, that would limit the mass assigned to the payload. Many reorientation techniques have been proposed over the years, the following are the most promising ones.

The first reorientation technique that has been studied for Mars parking orbits is the "Butterfly" maneuver. This method takes advantage of the third body effects, reorienting the spacecraft near the edge of Mars sphere of influence. This allows the maneuvers performed at such a large distance from the planet to be particularly inexpensive. The propulsion system brings the spacecraft from a 5-sol arrival parking orbit to the limit of Mars sphere of influence. Once there, a series of small maneuvers reorient the spacecraft before a larger burn brings it back to a 5-sol

departure parking orbit. The duration of this sequence ranges between 100 and 250 days, though the total  $\Delta V$  is relatively independent of it.

The second reorientation technique is the "Apotwist" reorientation. This method, introduced by Landau, consists of three maneuvers: a tangential capture burn into the arrival parking orbit, a single plane change at apoapsis that twists the orbit around its line of apsides, after a optimized portion of the total stay time, and a tangential escape burn into the hyperbolic interplanetary trajectory. The orbit precession during the stay time is used as a mean to reorient the spacecraft, as the plane change, the apotwist, takes place at an optimized time, so that the departure orbit will be correctly aligned for a tangential burn of escape.

The last reorientation technique is an evolution of the apotwist method and is called "Bi-elliptic Apotwist". This utilizes a sequence of seven burns to reorient the spacecraft from its arrival orbit to the departure one. This has been studied in detail in chapter 4, and a possible way to evaluate the optimized parameters for this method has been suggested, using as an optimization tool the MATLAB implementation of genetic algorithms.

# Chapter 2

## Genetic algorithms

As previously stated in chapter 1, the optimization of the parking orbits has been carried out with the MATLAB implementation of a genetic algorithm. In this chapter, the theory of genetic algorithms will be presented, with a special attention to the algorithm that has been used.

### 2.1 History of evolutionary and genetic algorithms

Evolutionary algorithms are biologically inspired tools for engineering optimization [7]. The development of these algorithms began in the 1950s, when numerous computer scientists independently started studying a way to use the classic Darwinian theory of evolution as a tool of optimization for biology and engineering problems [8]. The aim was to evolve a population of initial solutions to a given problem, through operators simulating natural selection. The principle of ‘survival of the fittest’, in which the best individual is able to survive among environmental and predators’ hazards and reproduce, is indeed comparable with the computational optimization of a large number of possible solutions. Genetic algorithms are the most widely utilized outcomes of these preliminary studies [9]. These are stochastic search and optimization methods [10].

The earliest evolutionary algorithms were probably developed by Alex Fraser, a biologist whose aim was to simulate the evolutionary process for controlled experiments. De facto, though, genetic algorithms (GAs) were created by John Holland, a computer scientist and psychologist at the University of Michigan, and developed by him and his students and colleagues in the 1970s. His book, published in 1975, *Adaptation in Natural and Artificial Systems*, presents genetic algorithms as a broadening of Darwinian evolution outside biology, that could be used to solve problems in various fields of application. Holland’s work serves as the foundation

of nearly all implementations of genetic algorithms to this day, even if present day algorithms can vary widely from his original concept. Holland's method was based on the idea of evolving a population of "chromosomes", consisting of "genes" made of "alleles", into a new one using the principle of survival of the fittest and the genetic operators of crossover, mutation and inversion. The algorithm selected the fittest chromosomes and allowed them to create a new generation of individuals, modified from the original through the genetic operators listed before. In particular, crossover function recombined genes of two different chromosomes, mimicking biological recombination; mutation varied the value of some alleles randomly; inversion swapped contiguous sections of the chromosome.

Thanks to the work of numerous scientists, genetic algorithms developed further in the 1980s and 1990s, finding their first engineering applications as optimization tools. They have since been used in very different fields, for example design and operation of pumping stations (Rasoulzadeh-Gharibdousti et al., 2011) and urban stormwater management (Montaseri et al., 2015) [11].

## 2.2 Terminology

Genetic algorithms terminology is borrowed from biology and used in close analogy to it, even if it acquires a much simpler meaning. The terminology is here listed:

- *chromosome*: possible solution to a given problem, generated by the GA and usually encoded as a bit string
- *gene*: block of adjacent bits that represent a particular element of the chromosome
- *allele*: each of the single bits that constitute genes
- *locus*: position of a gene inside the chromosome
- *population*: totality of chromosomes
- *parent*: chromosome that represents the old solution allowed to reproduce
- *offspring or children*: chromosomes generated by reproduction of two parent chromosomes, representing the new solutions
- *fitness function*: function that assigns a score to each chromosome in terms of quality of the solution: the higher the fitness function, the fittest the solution
- *elite*: fittest chromosomes, best solutions
- *generation*: each iteration of the algorithm

- *run*: entire set of generations
- *crossover*: genetic operator that exchange genes between two parents
- *mutation*: genetic operator that flips the bit of the offspring population at a randomly chosen locus

## 2.3 Genetic algorithm structure and characteristics

Genetic algorithms are flexible heuristic optimization methods, as they can be used in a vast range of problems. These algorithms mimic the evolutionary process, that allows the best individuals, that are able to adapt to the environment, to survive and mate, as much as the best solution to a problem is allowed to create a new and possibly better generation of solutions. Genetic algorithms fall into the category of computational intelligence, that classically subdivides into genetic algorithms, neural networks and fuzzy logic, that all aim to simulate human intelligence. Genetic algorithms can also successfully be used where other optimization methods fail due to difficult conditions of the problem.

In general, given the problem which solution is to be optimized, the structure of the algorithm can be summarized as:

1. Definition of an initial population of  $n$  chromosomes, possible solutions to the problem, usually randomly generated.
2. Fitness function evaluation of the current generation's chromosomes.
3. Selection of the fittest chromosomes to be parents (elite).
4. Reproduction of the parents and creation of a new generation of solutions (offspring) by applying crossover and mutation operators.
5. Iteration of the steps 2-4 until the stopping criteria are met and the optimized solution is found.

When the stopping criteria are met, the highest fit chromosome in the last generation represents the optimal solution to the problem. Due to the fact that the initial population is chosen at random, different runs can produce different optimal solution, as the evolution of the chromosomes follows a dissimilar path. The optimal solution, therefore, of the overall problem can be found after a large number of runs, or possibly can never be reached.

The algorithm scheme is shown in figure 2.1.

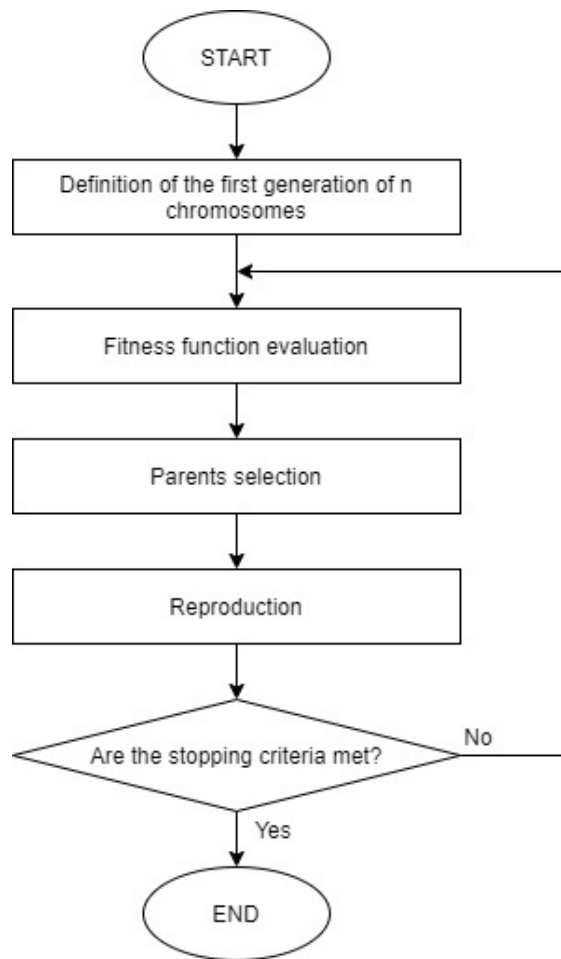


Figure 2.1: Genetic algorithm scheme

## 2.4 Creation of the initial population

Genetic algorithms need to work on an initial generation or population, from which the evolution and reproduction may begin. Each chromosome will be an  $1 \times N$  array, where  $N$  is the dimension of the given optimization problem, defined as:

$$\text{Chromosome} = X = (x_1, x_2, \dots, x_N) \quad (2.1)$$

where:

- $X$  is a solution to the optimization problem
- $x_i$  is the  $i$ th gene of the solution  $X$ , representing a decision variable
- $N$  is the total number of genes

The initial population, or the first generation, is generated by the genetic algorithm and it can be represented by a  $M \times N$  matrix of chromosomes,  $M$  being the number of chromosomes in the population:

$$Population = \begin{bmatrix} X_1 \\ X_2 \\ \vdots \\ X_j \\ \vdots \\ X_M \end{bmatrix} = \begin{bmatrix} x_{1,1} & x_{1,2} & \dots & x_{1,i} & \dots & x_{1,N} \\ x_{2,1} & x_{2,2} & \dots & x_{2,i} & \dots & x_{2,N} \\ \vdots & \vdots & & \vdots & & \vdots \\ x_{j,1} & x_{j,2} & \dots & x_{j,i} & \dots & x_{j,N} \\ \vdots & \vdots & & \vdots & & \vdots \\ x_{M,1} & x_{M,2} & \dots & x_{M,i} & \dots & x_{M,N} \end{bmatrix} \quad (2.2)$$

where:

- $X_j$  is the  $j$ th chromosome
- $x_{i,j}$  is the  $i$ th gene of the  $j$ th chromosome
- $M$  is the population size

The initial population should be chosen randomly to represent the whole solution space, in order to be able to evolve in as many directions as possible towards the optimized solution. Therefore, the population's size should be evaluated carefully.

In case the chromosome is a bit string, the initial population of dimension  $4 \times 6$  might look like table 2.1.

**Table 2.1:** Initial population example

Chromosome label	Chromosome string	Fitness Value
A	00100011	3
B	11011111	7
C	11000011	4
D	00001010	2

After the creation of the initial population, the fittest chromosomes are selected to be parents of the new generation. Each generation will have size  $M$ , as some chromosomes will reproduce more than once.

## 2.5 Fitness computation

The fitness function is the index of the quality of the solution each chromosome generated by the genetic algorithm represents or how well each chromosome solves the given problem. It is vital to evaluate it for every chromosome in the population

to understand which individuals are the fittest to survive, evolve and procreate. The fitness function has the form:

$$F = f(x_1, x_2, \dots, x_N) \quad (2.3)$$

where:

- $F$  is the value of the fitness function for a given chromosome
- $f$  is the fitness function
- $x_i$  is the  $i$ th gene of the given chromosome

As genetic algorithms can be applied to numerical problems, where the goal is to maximize or minimize the fitness function, but also to non-numerical problems, such as biological optimization, in which case the fitness function can be complex to evaluate, this function needs to be selected with attention, as it can compromise or enhance the functioning of the algorithm in toto. For example, as the evaluation of the fitness function for every chromosome of every generation takes up the majority of the computational run time of the algorithm, it is beneficial to minimize the number of fitness function calls until the optimum is reached. It has to be noted that the computational speed of the fitness function is also affected by the number of variables (chromosomes' genes) and constraints of the solution.

## 2.6 Parents selection

Once the value of the fitness function has been evaluated for each of the chromosomes of the current generation, the selection of the parents to carry out the reproduction process may begin. This selection implements Darwin's principle of survival of the fittest. The genetic algorithm selects  $R$  parent chromosome, with  $R < M$  (where  $M$  is the population size), that are considered the fittest to procreate an offspring that will progress towards the optimal solution. As already anticipated, the fitness function is the mean by which the selection operates. The most common selection methods are:

- Proportionate selection
- Rank selection
- Tournament selection

### 2.6.1 Proportionate selection

The proportionate selection method, also known as the “roulette-wheel selection”, was introduced by Goldberg in 1989 and states that the probability of a chromosome parental selection is:

$$P_k = \frac{F(X_k)}{\sum_{j=1}^M F(X_j)} \quad (2.4)$$

where:

- $P_k$  is the probability of the selection of the  $k$ th chromosome
- $X$  is the chromosome
- $F(X)$  is the fitness function of the chromosome  $X$

The cumulative probability for all chromosomes is:

$$Q_j = \sum_{k=1}^j P_k, \quad j = 1, 2, \dots, M \quad (2.5)$$

where:

- $Q_j$  is the cumulative probability of the  $j$ th chromosome

Based on the relative probability of the chromosomes normalized with the cumulative one, a roulette wheel is created and randomly spun to select parents, see figure 2.2 for a simple example case. The selection of  $R$  parents is achieved by spinning the wheel  $R$  times. As shown in the figure, each individual is given a slice of the roulette, proportionate to its fitness value. The selection will therefore be biased towards individuals with a higher fitness value, but any individual has a positive probability of becoming a parent. One of the possible issues with this method is that the fittest parents may as well never be selected, due to the random nature of the selection. Although apparently counter-active, this might be a mean to avoid local optima and proceed towards the global optimal solution. Disadvantages to this method are the possibility of premature convergence, in case one solution has a much higher fitness value than the rest, or, on the contrary, stagnation, when the differences of the fitness values are too small. The first case has a high selective pressure and low population diversity, while the second has a low selective pressure and a high population diversity.

Solution	Fitness function	Probability
1	60	0.5
2	40	0.33
3	20	0.17

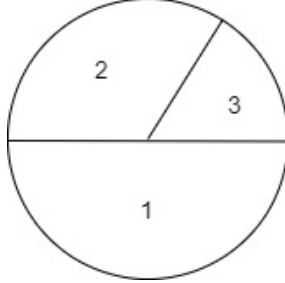


**Figure 2.2:** Proportionate selection scheme

## 2.6.2 Rank selection

Rank selection was devised by Baker in 1985. Its purpose is to prevent a too quick convergence to a solution, that would not reach to global optimum, or local optimum issues. In Baker's version, the chromosomes are ranked according to their fitness and the value of each individual is based on its rank, rather than the fitness function absolute value. The rank of the best solution is 1, while the worst solution receives rank  $M$ , the lowest one. Differently from the roulette wheel selection, there is no need to normalize the fitness value. Again, each solution will be assigned a probability of reproduction based on its rank. Here follows a common example of rank assignment:

$$P_k = U - (S_k - 1) \times Z \quad (2.6)$$

$$S_k = \text{Rank}(X_k) \quad (2.7)$$

$$\sum_{j=1}^M P_j = 1 \quad (2.8)$$

$$U = \frac{Z(M-1)}{2} + \frac{1}{M} \quad (2.9)$$

where:

- $S_k$  is the rank of the  $k$ th chromosome in the generation
- $Z$  is a value chosen by the user

Since the probability is based on rank, rather than fitness absolute value, this method guarantees an increased diversity in the offspring generations compared to fitness proportionate selection, that can result in a better overall optimization. On the contrary, there is the possible disadvantage of slowing down the selection pressure, leading to an overall slower genetic algorithm. These issues can be solved with attentive choices from the user, through the adjustment of the  $Z$  parameter:  $Z=0$  leads to no selective pressure, as all individuals have the same probability of selection, while increasing  $Z$  leads to higher selective pressure.

### 2.6.3 Tournament selection

A more time and computation efficient method than the previous two is the tournament selection. According to this method, a set of  $Y$  ( $1 < Y < M$ ) chromosomes is randomly selected from the current generation with uniform distribution. In this way every chromosome has the same probability of being selected. Within these  $Y$  individuals, the one with the highest fitness value is selected as a parent. The  $Y$  individuals are then returned to the original population to be potentially selected again. The process is iterated until enough parent individuals have been selected. The value of  $Y$  controls the selective pressure, as large values of  $Y$  increase the pressure. Typically, though, the value of  $Y$  is 2.

## 2.7 Reproduction

The genetic algorithm generates with each iteration a population of new individuals as offspring of the previous one. For the reproduction process, two computational operators, directly inspired by genetics, are used: crossover and mutation. After the mating selection of two individuals already designated as parents, their genes and alleles undergo crossover, with probability  $P_C$ . If parents do not cross over, their offspring are exact copies of each parent. Next, each child is subject to mutation of each allele with probability  $P_M$ . Again, the mutation may not happen, so the offspring may be identical to the parents. The offspring after mutation is the new generation. The reproduction process is shown in figure 2.3.

### 2.7.1 Crossover

The crossover operator allows the creation of new offspring by the combination of genes of usually two parents. Crossover can also be extended to more than two parents, modifying the genetic algorithm. The offspring genes are therefore part equal to one parent and part to the other. This operator imitates the biological exchange of genes between partners that their offspring inherits. The three main types of crossover, described by Goldberg (1989) and Michalewicz (1996), are:

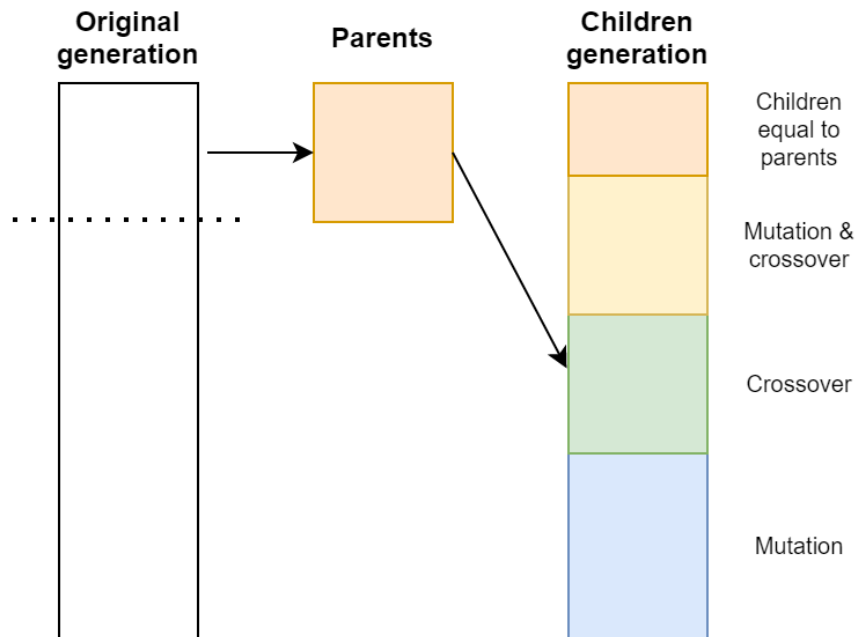


**Figure 2.3:** Reproduction scheme

- One-point crossover
- Two-point crossover
- Uniform crossover

Each of these methods is depicted in figure 2.4. The one-point crossover randomly selects a crossover point, as shown in figure 2.4. The first of the two children is created so that its genes are exactly those of one parent before the crossover point and those of the another parent after that point. The second child, is generated with the same logic, just inverting the two parents' genes. The two-point crossover operates in the way but selecting two points of crossover. The genes between these two points are maintained in the same position as the parent in the offspring, while the genes external to the two boundaries are exchanged. The uniform crossover randomly exchanges genes between parents to create the two children.

## 2.7.2 Mutation

The second genetic operator is the mutation. This mechanism is applied directly to the offspring generation and goes to introduce new genetic material to it. The mutation operator replaces randomly some of the genes or alleles of each child individual with a probability  $P_M$ . Mutation is applied to the genes of the

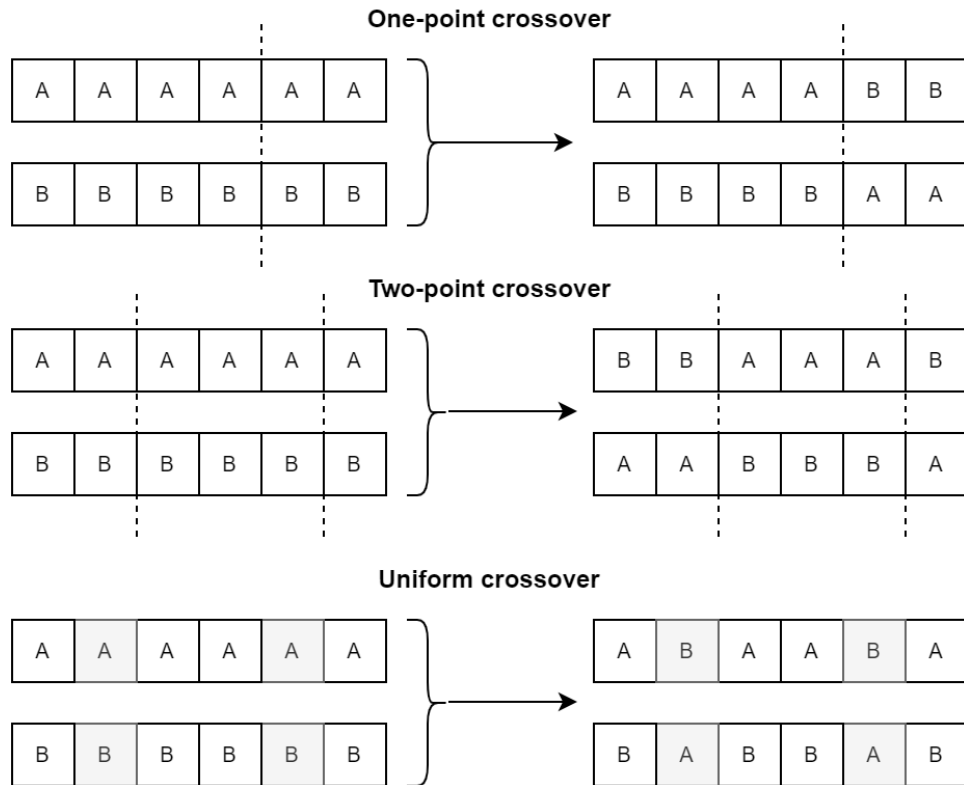


**Figure 2.4:** Different crossover methods scheme

chromosomes representing the children population, by generating a random number in the range  $[0,1]$  for each gene. If this number is less than  $P_M$ , that gene is mutated, otherwise it remains unchanged. The mutation process is displayed in figure 2.5.

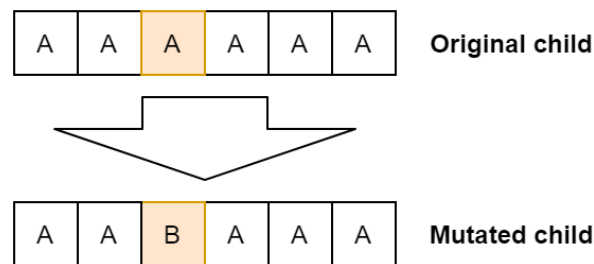


**Figure 2.5:** Mutation scheme

The two main methods of mutation for problems using real values are:

- Uniform mutation
- Nonuniform mutation

Uniform mutation replaces the gene that has been selected to mutate with a randomly generated gene within the feasible space of the solutions imposed by the user. Therefore, the mutated gene will have a random value between that variable lower and upper boundary. Let  $X$  and  $x_i$  be respectively the offspring chromosome and randomly chosen gene before mutation and  $X'$  and  $x_i'$  be the ones after mutation:

$$X = (x_1, x_2, \dots, x_i, \dots, x_N) \quad (2.10)$$

$$X' = (x_1, x_2, \dots, x_i', \dots, x_N) \quad (2.11)$$

$$x_i' = Rnd(x_i^{(L)}, x_i^{(U)}) \quad (2.12)$$

where:

- $x_i^L$  is the lower boundary for the  $i$ th gene
- $x_i^U$  is the upper boundary for the  $i$ th gene

Nonuniform mutation chooses a new value for the mutated gene in an increasingly localized space, as the lower and upper boundary of the feasible space of the solution narrows as the genetic algorithm iterates. The mutated gene has the form of:

$$x_i' = Rnd(x_i - d, x_i + d) \quad (2.13)$$

$$d = d_0 \times \frac{T - t}{T} \quad (2.14)$$

where:

- $d_0$  is the initial value of  $d$
- $t$  is the current iteration
- $T$  is the maximum number of iterations

Another possibility would be choosing the mutated value of the gene using a Gaussian probability distribution, therefore allowing the most statistically reasonable assumption to be the most probable.

## 2.8 Termination

The termination of the algorithm iterations takes place when the termination conditions are met. It is therefore fundamental to choose a good criterion to allow the correct convergence of the solutions. Some termination criteria may be:

- A predefined number of generations.
- Running time.
- Amount of improvement of the function to optimize between two consecutive generations, thus stagnation due to convergence of the optimization process.

The global optimum, though, may not have been reached, even after the termination of the algorithm. As stated previously, many runs of the same algorithm could bring the global optimum.

## 2.9 Genetic algorithms in MATLAB

A genetic algorithm is already implemented in MATLAB and is part of the Global Optimization Toolbox [12]. This toolbox provides different methods that search for global optimal solutions of problems characterized by multiple local maxima or minima. The MATLAB genetic algorithm solver, 'ga', is apt for smooth and non-smooth optimization, with the possibility of adding any type of constraints [13]. In particular, 'ga' finds the minimum of a given function using the principles of genetic algorithm detailed in the previous sections. The user's optimization options are expressed through the function 'optimoptions'.

The syntax to call the genetic algorithm in MATLAB is:

$$[x, fval, exitflag, output, population, scores] = \\ ga(fun, nvars, A, b, Aeq, beq, lb, ub, nonlcon, options)$$

There are also alternative ways to use this algorithm, but the form presented is one of the most complete and also the one that has been used in this thesis study. Every element of the call of the genetic algorithm is explained in table 2.2 [14].

The optimization options are expressed as a structure output of the 'optimoptions' MATLAB function. There are numerous options possibilities, regarding for example tolerance, population dimension, running time etc. A basic example of an option definition is the following:

**Table 2.2:** List of MATLAB GA elements

<i>x</i>	Local unconstrained minimum
<i>fval</i>	Value of the fitness function at <i>x</i>
<i>exitflag</i>	Integer identifying why the algorithm has stopped
<i>output</i>	Structure containing information about performance of the algorithm
<i>population</i>	Matrix of the final population
<i>scores</i>	Scores of the final population
<i>fun</i>	Objective function
<i>nvars</i>	Number of decision variables, genes. Dimension of the problem
<i>A</i>	Linear inequality matrix, $A * x \leq b$
<i>b</i>	Linear inequality vector, $A * x \leq b$
<i>Aeq</i>	Linear equality matrix, $A_{eq} * x = b_{eq}$
<i>beq</i>	Linear equality vector, $A_{eq} * x = b_{eq}$
<i>lb</i>	Set of lower bounds
<i>ub</i>	Set of upper bounds
<i>nonlcon</i>	Non-linear constraints
<i>options</i>	User defined optimization options

*options* = *optimoptions*('ga', *PlotFcn*, @*gaplotbestf*)

In table 2.3 some of the most common options are listed and briefly described. In particular, all the options that have been used in the work of this thesis are presented.

**Table 2.3:** List of possible user options for MATLAB GA

<i>CrossoverFcn</i>	Function that is used to crossover the parents genes
<i>CrossoverFraction</i>	Fraction of the offspring population subject to crossover
<i>Display</i>	Level of display
<i>EliteCount</i>	How many chromosomes of the current generation survive into the next one
<i>FunctionTolerance</i>	Tolerance in the average fitness value change over two consecutive generations
<i>InitialPopulationMatrix</i>	Initial population given as an input
<i>InitialPopulationRange</i>	Range of values of the first generation
<i>MaxGenerations</i>	Maximum number of iterations
<i>MaxTime</i>	Maximum running time
<i>MigrationDirection</i>	Preferred direction of migration
<i>MutationFunction</i>	Function that is use to mutate the offspring genes
<i>PlotFcn</i>	Function that plot output data
<i>PopulationSize</i>	Size of the population, M
<i>SelectionFcn</i>	Function that selects parent chromosomes

# Chapter 3

## Physical model

### 3.1 Laws controlling orbital mechanics

The basis to modern orbital mechanics lays in the works of many astronomers and scientists. The most notable works belong to Kepler and Newton, whose studies allowed the development of the discipline up until today's state of art. Johann Kepler, studying Tycho Brahe data from the observations of the motion of Mars, was able to develop his three laws of planetary motion [15]:

1. The orbit of each planet is an ellipse, with the Sun at one focus.
2. The line joining the planet to the Sun sweeps out equal areas in equal times.
3. The square of the period of a planet is proportional to the cube of its mean distance from the Sun.

Kepler's work, though still fundamental to the study of astronomical objects motion, was only a kinematic description and it still didn't solve the dynamic aspects of the motion [16]. Isaac Newton was the one to give it a solution, with his three laws of motion, detailed in Book I of his *Principia*:

1. Every body continues in its state of rest or of uniform motion in a straight line, unless it is compelled to change that state by forces impressed upon it.
2. The rate of change of momentum is proportionate to the force impressed and is in the same direction as that force.
3. To every action there is always opposed an equal reaction.

The second law of Newton is notoriously expressed as:

$$\vec{F} = m\vec{a} \tag{3.1}$$

where  $\vec{F}$  is the sum of all external forces acting on the body,  $m$  is the body mass and  $\vec{a}$  is the acceleration of the body.

Newton also introduced the Law of Universal Gravitation. This law describes the mutual forces acting that attract two bodies. It states that two given bodies attract one another with a force directed on the line joining the two, that is proportional to the product of their masses and inversely proportional to the square of their distances. This law has expression:

$$\vec{F}_g = -\frac{GMm}{r^2} \frac{\vec{r}}{r} \quad (3.2)$$

where  $\vec{F}_g$  is the gravitational force,  $M$  and  $m$  are the two bodies masses, and  $\vec{r}$  is the vector from  $m$  to  $M$ .  $G$  has the value of  $6.67 * 10^{-11} \frac{m^3}{kg s^2}$ .

## 3.2 The two-body problem

The two-body problem is a simplification of the N-body problem, that studies the gravitational forces among N bodies. This simplification is used as the physical model throughout this chapter and the following. It is based on Newton laws of motion, especially the second one (3.1), and on the universal law of gravitation (3.2), combined with Kepler's laws.

The two-body problem is based on the following assumptions:

- The two bodies are spherically symmetric with uniform density, therefore can be treated as a point mass.
- The only forces acting on the two bodies are gravitational.
- The mass  $m$  (the spacecraft) is negligible compared the mass  $M$  (the planet, or attracting body)
- The coordinate system chosen is inertial

Considering an inertial reference frame, illustrated in figure 3.1, and solving Newton's equations, the equation of relative motion of the spacecraft to the planet can be expressed as:

$$\ddot{\vec{r}} = -\frac{\mu}{r^2} \frac{\vec{r}}{r} \quad (3.3)$$

where  $\mu$  is the gravitational parameter, defined as:

$$\mu = GM \quad (3.4)$$

For Earth  $\mu$  is equal to about  $398\,633 \frac{km^3}{s^2}$ , while for Mars it is equal to approximately  $42\,828 \frac{km^3}{s^2}$ .

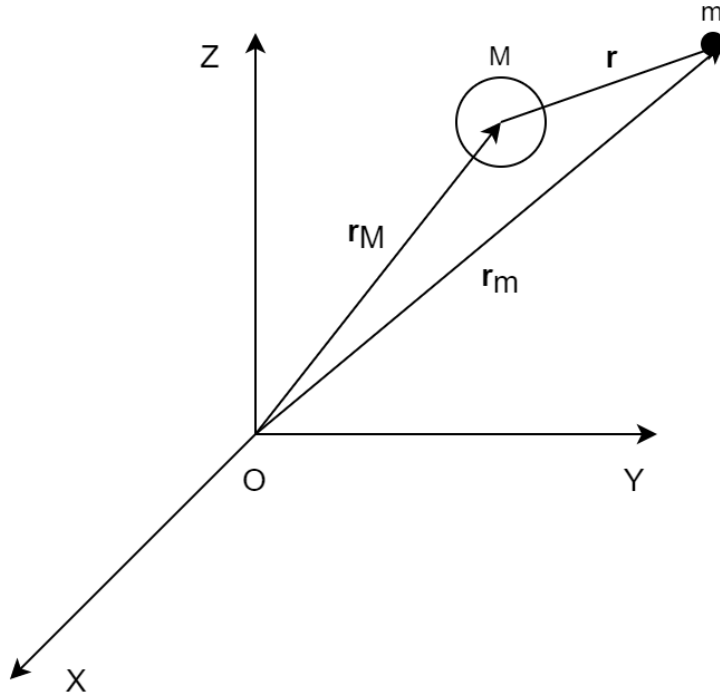


Figure 3.1: Two-body problem

### 3.2.1 Constants of motion

As the only forces applied to the two masses of the problem are gravitational, the field in which these forces operate is the gravitation field. This is a conservative field and thus there is conservation of the mechanical energy. In fact, a mass, only subject to gravity, moves without losing or gaining mechanical energy. The mass can only exchange kinetic energy for potential energy, and vice-versa. Therefore, mechanical energy is a constant of motion, unless an external force acts on the body. The specific mechanical energy per unit mass has expression:

$$\mathcal{E} = \frac{V^2}{2} - \frac{\mu}{r} \quad (3.5)$$

where the first term is the kinetic energy per unit mass and the second one is the potential energy per unit mass.

The other constant of motion is the specific angular momentum. The conservation of the angular momentum descends from the fact that without a tangential component of force, the angular momentum of a rotating system will not vary. Since gravitational forces are directed radially, on the line joining the two bodies, the angular momentum should not change. This is actually the case, as it can be

proven that the specific angular momentum is constant for the motion of a given mass around a much more massive body. This vector quantity can be expressed as:

$$\vec{h} = \vec{r} \times \vec{V} \quad (3.6)$$

It can be seen from its expression that  $\vec{h}$  will be perpendicular to the plane in which  $\vec{r}$  and  $\vec{V}$  lay. Since  $\vec{h}$  is constant as a vector, other than only its magnitude, the position vector and the velocity vector always lay on that same plane. This plane will be the orbital plane. The magnitude of  $\vec{h}$  can be evaluated as:

$$h = rV \cos \phi \quad (3.7)$$

where  $\phi$  is the flight path angle, displayed in figure 3.2, namely the angle between the local horizontal plane and the velocity vector. This has the same sign as  $\vec{r} \cdot \vec{V}$ .

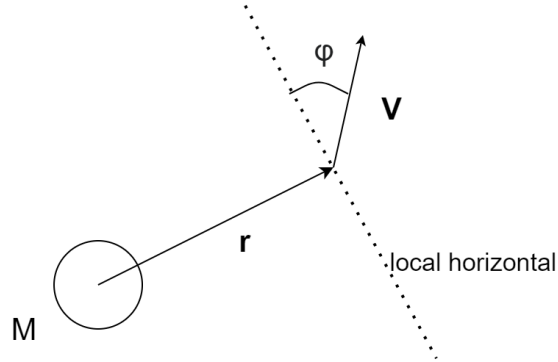


Figure 3.2: Flight path angle

### 3.3 Trajectory Equation

The trajectory equation derives from integration of the formulation of the relative motion expressed in (3.3) and goes to confirm the first law of Kepler, that states that each planet orbits around the Sun on an elliptical trajectory. After the integration, the solution for the position is:

$$r = \frac{h^2/\mu}{1 + \frac{B}{\mu} \cos \nu} \quad (3.8)$$

where  $B$  is the magnitude of the constant vector  $\vec{B}$ , that derives from the integration of the motion, while  $\nu$  is the angle between  $\vec{B}$  and the position vector  $\vec{r}$ .

The equation (3.8) can be recognized as the polar expression of a conic section:

$$r = \frac{p}{1 + e \cos \nu} \quad (3.9)$$

where  $p$  is a geometrical constant of conic sections called semi-latus rectum,  $e$  is the eccentricity, another constant for conic sections, and  $\nu$  takes the name of true anomaly.

Therefore, the first law of Kepler is confirmed, but extended: not only ellipses represent the solution to the trajectory of a mass in motion in a gravitational field, but also other conic sections, thus circles, parabolas and hyperbolas.

### 3.4 Conic sections geometry

A conic section is the curve obtained with the intersection of a plane and a cone (Fig. 3.3). The only conic section that does not represent the motion of a spacecraft in a gravitational field, is the point at the intersection of the two halves of the cone. Rectilinear orbits, that represent the ideal limit of parabolic and hyperbolic orbits, are also conic sections, resulting from the intersection of the cone and a plane parallel to it.

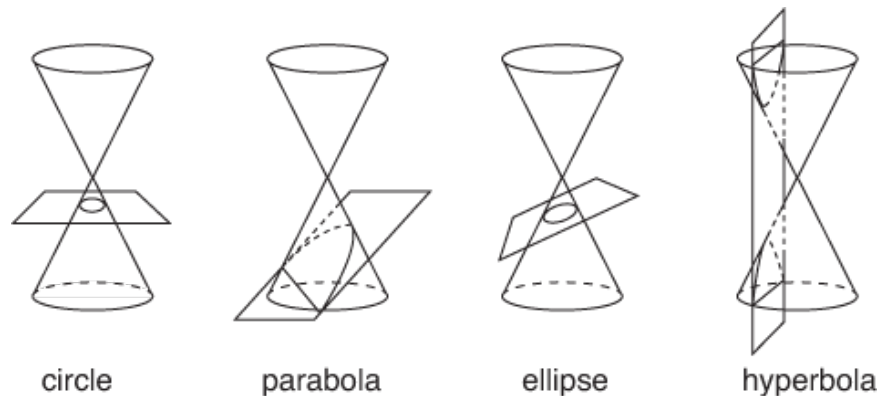


**Figure 3.3:** Conic sections

A different but equivalent definition of conic section can be the following: "A conic is a circle or the locus of a point which moves so that the ratio of its absolute distance from a given point (a focus) to its absolute distance from a given line (a directrix) is a positive constant  $e$  (the eccentricity) [15]." In regard with the ellipse, figure 3.4 displays these elements.

While the directrix and the secondary focus  $F'$  hold little to no physical meaning in the study of orbits, on the contrary, both the prime focus  $F$  and the eccentricity  $e$  are fundamental. In particular, the main attracting object is located in the focus

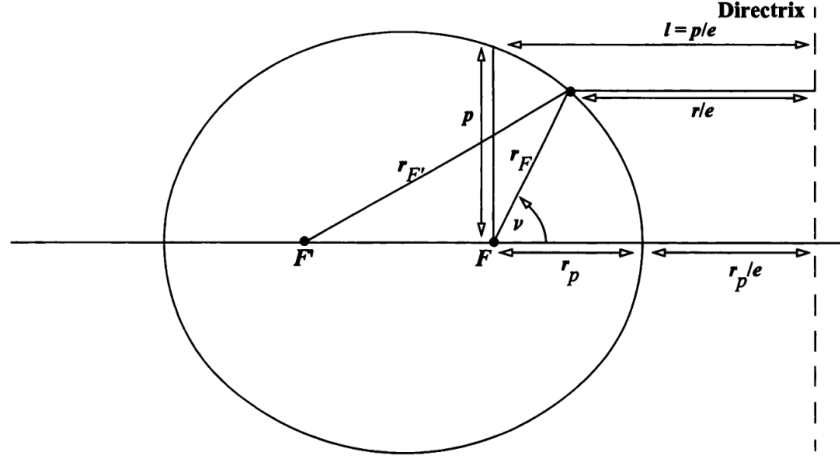


**Figure 3.4:** Elements of a conic section [16]

and the eccentricity determines the type of orbit and its shape. For any conic section, it is mathematically proven that:

$$\begin{aligned} r_{F'} + r_F &= \text{constant} = 2a \\ |r_{F'} - r_F| &= \text{constant} = 2c \end{aligned} \quad (3.10)$$

where  $r_F$  is the distance from the main focus  $F$  to a given point of the conic section and  $r_{F'}$  is the distance from the secondary focus  $F'$  to the same given point of the conic section.  $r_F$  will be now forward called  $r$ .

The eccentricity is:

$$e = \frac{c}{a} \quad (3.11)$$

where  $c$  is the semi-distance between the two foci  $F$  and  $F'$  and  $a$  is the semi-major axis.

The semilatus rectum, already briefly introduced in equation (3.9), is detailed graphically in figure 3.4. Its expression is:

$$p = a(1 - e^2) \quad (3.12)$$

It is now possible to find the expression to the periapsis radius, combining equation (3.9) with the expression of the semilatus rectum (3.12), knowing that at periapsis the angle  $\nu = 0^\circ$  (fig. 3.4). The radius at periapsis is also the minimum, the closest point to the main focus.

$$r_P = \frac{p}{1 + e} = a(1 - e) \quad (3.13)$$

In the same way, the radius at apoapsis, where  $\nu = 180^\circ$ , is found:

$$r_A = \frac{p}{1 - e} = a(1 + e) \quad (3.14)$$

### 3.4.1 Relating orbit geometry and constants of motion

Comparing equation (3.8) and equation (3.9), it is clear that the eccentricity vector is equal to:

$$\vec{e} = \frac{\vec{B}}{\mu} \quad (3.15)$$

The vector  $\vec{B}$  points in the direction of the periapsis, therefore towards  $\nu = 0^\circ$ . Integrating the equation of motion (3.3) and solving for  $\vec{B}$ , the eccentricity vector can be expressed in function of  $\vec{r}$ ,  $\vec{V}$  and  $\vec{h}$  as follows:

$$\vec{e} = \frac{\vec{V} \times \vec{h}}{\mu} - \frac{\vec{r}}{r} \quad (3.16)$$

Furthermore, from the comparison of the two expressions for the trajectory equation, the semilatus rectum depends on the value of the specific angular momentum magnitude:

$$p = \frac{h^2}{\mu} \quad (3.17)$$

It is also possible to relate the mechanical energy to the conic elements. In particular, writing the energy equation (3.5) at periapsis, it is found that the mechanical energy has the following expression:

$$\mathcal{E} = -\frac{\mu}{2a} \quad (3.18)$$

This equation is valid for all orbits and tells that the semi-major axis depends only on the specific mechanical energy, which is constant across the whole orbit. In the same way, the specific mechanical energy value gives information on the type of orbit:

- $\mathcal{E} < 0$  for a closed orbit, thus either a circle or an ellipse.
- $\mathcal{E} = 0$  for a parabolic orbit.
- $\mathcal{E} > 0$  for a hyperbolic orbit.

Equating equation (3.5) and equation (3.18), the following relation, which is valid for every orbit along its entire course, is found:

$$\frac{V^2}{2} - \frac{\mu}{r} = -\frac{\mu}{2a} \quad (3.19)$$

### 3.4.2 Elliptical orbits

The vast majority of spacecraft orbits are closed, therefore circular or elliptical. Circular orbits can be seen as a particular case of elliptical ones, where the semi-major axis and the semi-minor axis coincide and are the radius.

The semi-major axis expression is derived from (3.10), valid for all conic sections, and relates the radius of periapsis and apoapsis:

$$a = \frac{r_P + r_A}{2} \quad (3.20)$$

The eccentricity can also be expressed in terms of these two radii, since (3.11), as:

$$e = \frac{r_a - r_P}{r_A + r_P} \quad (3.21)$$

Since the elliptical orbit is a closed one, it is possible to determine the orbital period, which goes to confirm Kepler's third law: "The square of the period of a planet is proportional to the cube of its mean distance from the Sun". The orbits of planets around the Sun are indeed elliptical and the mean distance is  $a$ , as shown in equation (3.20). The period of the elliptical orbit is:

$$\mathcal{T} = 2\pi \sqrt{\frac{a^3}{\mu}} \quad (3.22)$$

It is clear that this quantity depends uniquely on the size of the orbit, through the semi-major axis, rather than in shape.

### 3.4.3 Hyperbolic orbits

Hyperbolic orbits describe the path of interplanetary probes, within the Earth and the target planet gravitational field. They are orbits that allow the spacecraft to escape the planet's gravitational influence with a velocity larger than zero. Therefore this velocity is imagined to be the velocity of the spacecraft at an infinite

distance from the planet. Said velocity, called hyperbolic excess speed, can be computed from the energy equation (3.19), as:

$$V_{\infty}^2 = V_{BO}^2 - \frac{2\mu}{r_{BO}} = V_{BO}^2 - V_{esc}^2 \quad (3.23)$$

where  $V_{BO}$  and  $r_{BO}$  are respectively the velocity and the position radius at burn out.  $V_{esc}$  is the escape velocity, the velocity needed to escape the gravitational field of a planet with zero velocity (parabolic orbit).

The theoretical "infinite distance" identifies the sphere of influence. This is an imaginary sphere drawn around every gravitational central body to delimit the space within which this central body is the primary gravitational influence on the probe. The sphere of influence is a concept rather than a physical notion, therefore there are different definition for it.

## 3.5 Coordinate systems

It is necessary to define an inertial reference frame, in which to study the optimization of the Mars parking orbits. In particular, three reference frame systems are useful to this study, and those are:

- The Equatorial Coordinate System
- The Right Ascension-Declination System
- The Perifocal Coordinate System

To define a reference frame system, a few elements are needed:

- Position of the origin
- Orientation of the fundamental plane
- Principal direction
- Positive direction of the Z-axis

### 3.5.1 The Equatorial Coordinate System

The Equatorial Coordinate System is also know as 'Geocentric', when it is applied to the Earth. It is valid, though, even in consideration with any other planet, in this specific case Mars. The unit vectors representing the three axis X,Y and Z are  $\hat{I}$ ,  $\hat{J}$  and  $\hat{K}$  respectively. This reference frame is the most used in chapter 4, as orbital elements evaluation is based on it.

The Equatorial Coordinate System has its origin in the center of the planet. The fundamental plane, where X and Y lay, is the equator, and X-axis points towards the vernal equinox direction, therefore the Aries Constellation. Z-axis positive direction is towards the North pole. This reference frame is non-rotating in respect with the fixed stars.

The unit vectors are obviously defined as:

$$\hat{I} = \begin{bmatrix} 1 \\ 0 \\ 0 \end{bmatrix} \quad (3.24)$$

$$\hat{J} = \begin{bmatrix} 0 \\ 1 \\ 0 \end{bmatrix} \quad (3.25)$$

$$\hat{K} = \begin{bmatrix} 0 \\ 0 \\ 1 \end{bmatrix} \quad (3.26)$$

### 3.5.2 The Right Ascension-Declination System

The Right Ascension-Declination reference frame is closely related to the Equatorial one, presented in the previous section. It is a polar system that can be identified with a celestial sphere of infinite radius. The origin of the system is in the center of said sphere and the fundamental plane is the celestial equatorial plane. These two can be superposed with the Equatorial Coordinate System. Therefore, the origin can be the center of a planet and the fundamental plane can be the planet equatorial plane. The X-axis is still the direction of the vernal equinox and the positive direction of the Z-axis is still the hemisphere containing Polaris or equivalently the North Pole.

The position of the body is described by three parameters: the distance from the reference origin  $r$ , the right ascension angle  $\alpha$ , measured eastward from the vernal equinox direction (the X-axis), and the declination angle  $\delta$ , measured northward from the celestial equator.

The coordinate in this reference frame are expressed as:

$$\vec{r} = \begin{Bmatrix} x \\ y \\ z \end{Bmatrix} = \begin{Bmatrix} r \cos \delta \cos \alpha \\ r \cos \delta \sin \alpha \\ r \sin \delta \end{Bmatrix} \quad (3.27)$$

Therefore, the right ascension and the declination can be found from the knowledge of the position of the spacecraft.

$$\alpha = \arctan\left(\frac{y}{x}\right) \quad (3.28)$$

$$\delta = \arcsin\left(\frac{z}{r}\right) \quad (3.29)$$

### 3.5.3 The Perifocal Coordinate System

One of the most useful coordinate systems is the Perifocal one. This is proper to every orbit, as its fundamental plane is the orbital plane itself. Its origin is the main focus of the conic section, therefore the center of the planet or mass to which the orbit is referred, the X-axis points in the direction of the periapsis and the Z-axis points in the direction of the vector  $\vec{h}$ , the specific angular momentum. The Y-axis is defined as perpendicular to X and contained in the orbital plane and is the direction of the semilatus rectum  $p$ . The unit vectors referred to the X, Y and Z axis are  $\hat{p}$ ,  $\hat{q}$  and  $\hat{w}$  respectively.

The position vector in the Perifocal Coordinate System has expression:

$$\vec{r}_{pqw} = \begin{Bmatrix} r \cos \nu \\ r \sin \nu \\ 0 \end{Bmatrix} \quad (3.30)$$

The velocity vector is:

$$\vec{V}_{pqw} = \begin{Bmatrix} -\frac{\mu}{h} \sin \nu \\ \frac{\mu}{h} (e + \cos \nu) \\ 0 \end{Bmatrix} \quad (3.31)$$

## 3.6 Classical orbital elements

The classical orbital elements are six independent quantities that can be used to unequivocally define an orbit and the position of the satellite along the orbit. These elements describe the type of conic section representing the orbit, its size and its three-dimensional orientation, in regard with the Equatorial Coordinate System, IJK. The six elements listed below are the most commonly used, but there exist variations to them, used in case of particular orbits that require them. The classical orbital elements are:

1. Semi-major axis  $a$ , a constant parameter, already previously defined, that gives information about the size of the conic section that describes the orbit.
2. Eccentricity  $e$ , a constant describing the type and shape of the orbit.
3. Inclination  $i$ , the angle between the unit vector  $\hat{K}$  (3.26) and the specific angular momentum vector  $\vec{h}$  (3.6).

4. Longitude of the ascending node  $\Omega$ , the angle between the unit vector  $\hat{I}$  (3.24) and the ascending node unit vector, measured eastward.
5. Argument of periapsis  $\omega$ , the angle between the ascending node vector and the periapsis direction, measured in the direction of the satellite's motion.
6. True anomaly  $\nu$  a time  $t$ , the angle between the periapsis direction at the position of the satellite at the time  $t$ , measured in the direction of the satellite's motion.

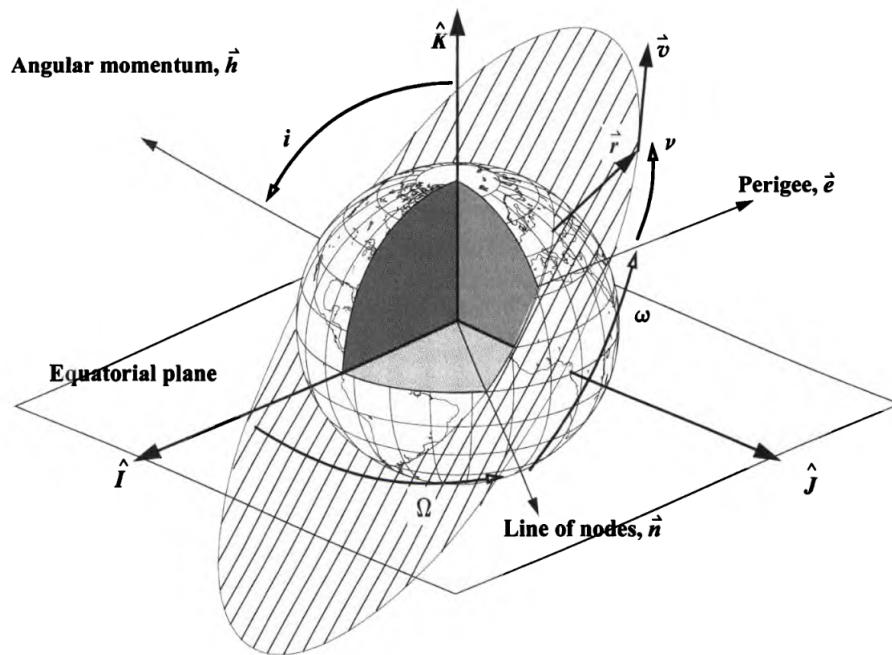


Figure 3.5: Classical orbital elements [16]

### 3.6.1 Determination of the orbital elements from position and velocity vectors

Knowing the position vector  $\vec{r}$  and the velocity vector  $\vec{V}$  at any given time in IJK reference frame, it is possible to find the six orbital elements, thus completely identifying the orbit.

The specific angular momentum is one of the quantities necessary to determine the orbital elements and has already been expressed as (3.6). The node unit vector,

which is the unit vector pointing from the origin to the ascending node, is defined as:

$$\hat{n} = \frac{\hat{K} \times \vec{h}}{|\hat{K} \times \vec{h}|} \quad (3.32)$$

The ascending node is the point where the satellite crosses the equatorial plane northward. The node unit vector, due to its definition, lies on the intersection of the equatorial plane and the orbital plane, called lines of nodes.

The last quantity needed to determine all the orbital elements that can be found from the knowledge of  $\vec{r}$  and  $\vec{V}$  is the eccentricity vector  $\vec{e}$ , which expression has already been found in (3.16).

The semi-major axis  $a$  can be found in various ways. One way is find  $a$  from the expression of energy (3.19) or from the expression of the semilatus rectum (3.12), which expression is directly found with the magnitude of the specific angular momentum (3.17).

The eccentricity  $e$  is found from the eccentricity vector, as:

$$e = |\vec{e}| \quad (3.33)$$

The inclination, namely the angle between  $\hat{K}$  and  $\vec{h}$ , has the expression:

$$i = \arccos \left( \frac{\hat{K} \cdot \vec{h}}{Kh} \right) \quad (3.34)$$

with:

- $0 \leq i \leq \pi$

The longitude of the ascending node, which is the angle between  $\hat{I}$  and  $\hat{n}$ , can be evaluated as:

$$\Omega = \arccos (\hat{I} \cdot \hat{n}) \quad (3.35)$$

with

- $0 \leq \Omega \leq \pi$  if  $n_Y > 0$
- $\pi < \Omega < 2\pi$  if  $n_Y < 0$

The argument of periapsis, which is the angle between  $\hat{n}$  and  $\hat{p}$ , as defined in the Perifocal Coordinate System, is:

$$\omega = \arccos (\hat{n} \cdot \hat{p}) \quad (3.36)$$

with

- $0 \leq \omega \leq \pi$  if  $p_Z > 0$
- $\pi < \omega < 2\pi$  if  $p_Z < 0$

Finally, the true anomaly, is defined as:

$$\nu = \arccos\left(\frac{\vec{e} \cdot \vec{r}}{er}\right) \quad (3.37)$$

with

- $0 \leq \nu \leq \pi$  if  $\vec{r} \cdot \vec{V} > 0$
- $\pi < \nu < 2\pi$  if  $\vec{r} \cdot \vec{V} < 0$

# Chapter 4

## Optimization study

### 4.1 The bi-elliptic apotwist technique

A round-trip mission to Mars, whether manned or unmanned, presents a great number of engineering challenges in all fields of the mission architecture. In particular, the focus of this thesis is on transportation system, that has to allow the spacecraft Mars capture and escape. The choice of parking orbits is crucial, as it impacts the  $\Delta V$  requirements, thus the total mass of the spacecraft and the mission as a whole.

The bi-elliptic apotwist technique, introduced by Qu, Merrill, Chai and Komar, for the optimization of Mars parking orbits offers a solution to satisfy the transportation system design requirements [17]. This method optimizes the Mars parking orbits using a seven burns strategy, that is more efficient than a much simpler two tangential burns technique (capture and escape burns). Given the conditions of the hyperbolic trajectories of capture and escape from Mars sphere of influence, the total  $\Delta V$  can be minimized both for hybrid and chemical propulsion. Furthermore, this technique can be adapted to many different missions and constraints, for example to land on planned sites, to transfer to and from Phobos and Deimos, Mars satellites, or to select a broad range of possible parking orbits.

The apotwist technique was first introduced by Landau. This consisted of a three burns sequence of an off tangential capture burn, a reorientation with a plane change at apoapsis burn, the apotwist, and an off tangential escape burn. Orbit precession due to perturbations is also taken in consideration and actually used as a mean to make the apotwist happen at an optimized moment. The bi-elliptic apotwist method is an evolution of Landau's sequence.

The bi-elliptic apotwist solution can be described as follows. The spacecraft approaches Mars on the capture hyperbolic orbit A. The first burn, performed near the periapsis of the hyperbole, transfers the spacecraft into a first bi-elliptic

transfer orbit B with an non-tangential maneuver. Once at apoapsis of orbit B, the second burn changes the orbit plane, bringing the spacecraft into orbit C, the second bi-elliptic transfer orbit. The spacecraft transfers to periapsis of orbit C and performs the third burn, which lowers the height of the apoapsis, finally inserting into the parking orbit D. Orbit D precesses due to orbit perturbations into orbit E during a portion of the total stay time, called twist time, when the spacecraft performs another plane change, the so called apotwist, with the fourth burn at apoapsis, transferring the spacecraft onto orbit F. Orbit F then precesses for the remaining stay time into orbit G, which is the departing parking orbit. The last three burns mirrors the first three. In fact, the fifth burn occurs at orbit G periapsis, and raises the height of the apoapsis, to the bi-elliptic transfer orbit H. At orbit H apoapsis the sixth burn changes the orbital plane into orbit I, the inbound transfer orbit. Finally, near orbit I periapsis, the seventh burn takes place, inserting the spacecraft into the hyperbolic escape orbit J, with another non-tangential maneuver [6]. The seven burns are summarized in table 4.1 and figure 4.1.

**Table 4.1:** Summary of the seven burns of the bi-elliptic apotwist

$\Delta V_1$ (A→B)	Insertion from hyperbolic capture orbit into bi-elliptical transfer orbit
$\Delta V_2$ (B→C)	First plane change at apoapsis
$\Delta V_3$ (C→D)	Apoapsis height change
Perturbations (D→E)	Perturbations propagation
$\Delta V_4$ (E→F)	Second plane change at apoapsis
Perturbations (F→G)	Perturbations propagation
$\Delta V_5$ (G→H)	Apoapsis height change
$\Delta V_6$ (H→I)	Third plane change
$\Delta V_7$ (I→J)	Insertion into the escape hyperbolic orbit

In this thesis study, the bi-elliptic technique has been combined with Cornick and Seversike method [18] for non-coplanar, non-tangential and off-periapsis capture and escape burns. In this way, it is possible to further reduce the cost of these two maneuvers and therefore the overall cost of the mission in terms of  $\Delta V$ . In fact, a coplanar maneuver can be accomplished only when the hyperbolic asymptote and the orbital plane are in the same plane and this is very restrictive for mission planning and can increase the mission cost. A tangential and at periapsis burn, obviously, only further raises the capture and escape burns cost.

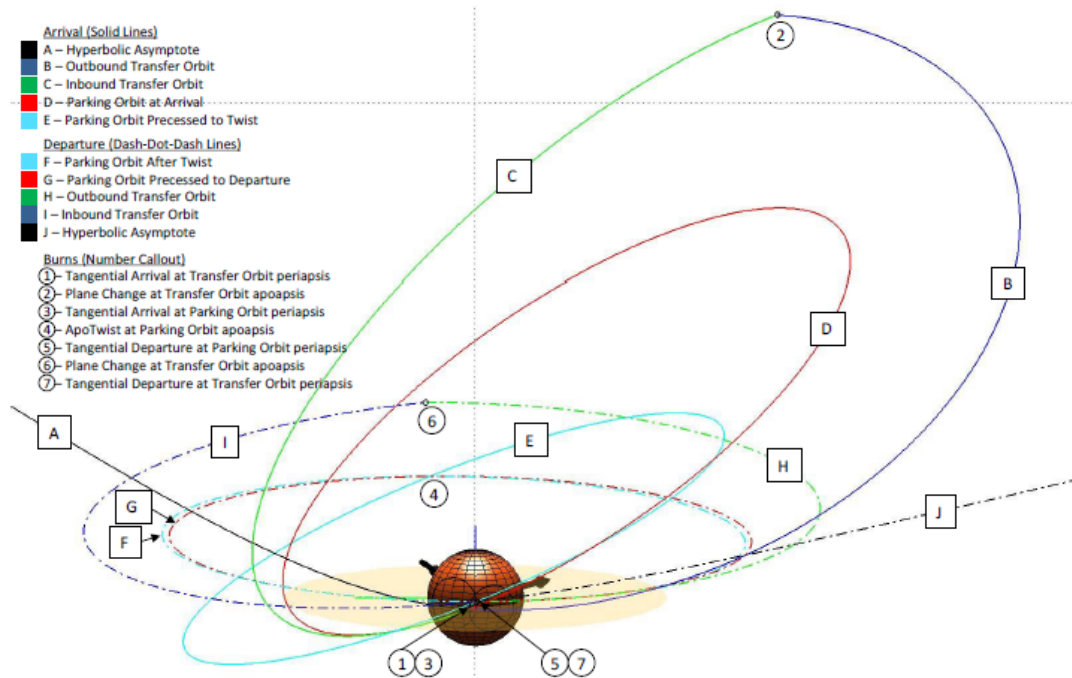


Figure 4.1: Bi-elliptic apotwist representation [6]

## 4.2 Methodology

To optimize the overall  $\Delta V$  cost of the seven maneuvers a MATLAB code has been implemented, using in particular a genetic algorithm to do so. As introduced in chapter 2, genetic algorithms always provide a solution, but have the drawback of never knowing if said solution is the overall optimum, or just a local optimal condition. Several runs are needed to unsure the solution is optimized.

To operate and compute the overall cost of the capture, escape and reorientation maneuvers, the genetic algorithm needs some parameters to describe the problem as inputs, such as the characteristics of the hyperbolic orbits of arrival and departure, the requirements for the parking orbit D and the total stay time on Mars. The code finds the value of some independent optimization variables, optimized to allow the minimum total  $\Delta V$ .

The parameters passed to the code as an input are summarized in table 4.2, while the algorithm optimized variables are summarized and described in table 4.3. The input parameters are constants within the problem, and are primarily needed to define it. The optimization variables are a set of independent variables that are chosen to uniquely find a solution to the given problem and fully describe the

different parking orbits.

**Table 4.2:** Optimization algorithm input parameters

Input Parameters	
$C_{3capt}$ [ $\frac{km^2}{s^2}$ ]	Capture hyperbolic orbit energy
$\alpha_{capt}$ [ $rad$ ]	Capture hyperbolic asymptote right ascension
$\delta_{capt}$ [ $rad$ ]	Capture hyperbolic asymptote declination
$C_{3esc}$ [ $\frac{km^2}{s^2}$ ]	Escape hyperbolic orbit energy
$\alpha_{esc}$ [ $rad$ ]	Escape hyperbolic asymptote right ascension
$\delta_{esc}$ [ $rad$ ]	Escape hyperbolic asymptote declination
$t_{stay}$ [ $days$ ]	Total stay time on Mars
$i_{PO}$ [ $rad$ ]	Parking orbit inclination
$r_P$ [ $km$ ]	Periapsis radius
$a_{bi-el}$ [ $km$ ]	Bi-elliptic transfer orbit semi-major axis
$a_{PO}$ [ $km$ ]	Parking orbit semi-major axis

**Table 4.3:** Optimization variables

Optimized output parameters	
$\omega_B$ [ $rad$ ]	Argument of periapsis of the bi-elliptical transfer orbit B
$\Omega_B$ [ $rad$ ]	Longitude of ascending node of the bi-elliptical transfer orbit B
$\nu_{capt}$ [ $rad$ ]	True anomaly of the bi-elliptic transfer orbit at capture burn
$\nu_{esc}$ [ $rad$ ]	True anomaly of the bi-elliptic transfer orbit at escape burn
$i_B$ [ $rad$ ]	Inclination of orbit B, the first bi-elliptic transfer orbit
$i_F$ [ $rad$ ]	Inclination of orbit F, after the second plane change
$i_I$ [ $rad$ ]	Inclination of orbit I, after the third plane change
$t_{DE}$ [ $days$ ]	Portion of the total stay time in which orbit D precesses into E

Some of the optimization variables could be user defined, other than the ones presented as inputs, to fulfill different mission requirements, not presented in this thesis. In the same way, some input parameters could be optimized by the algorithm, for example the semi-major axes of the bi-elliptic transfer orbit and of the parking orbit.

### 4.3 Analytical Development

All the following considerations use the physical model detailed in chapter 3. In particular, the following assumptions are valid in the analytical study:

- The two body problem represents the physical model. Therefore, the only gravitational influence on the spacecraft is Mars.
- The different maneuvers are impulsive.
- The reference frame that has been used is the Equatorial Coordinate System.
- The variables have been optimized as continuous, including the precession times from orbit D to orbit E and from orbit F to orbit G, even if the apotwist maneuver can occur only once per revolution, at apoapsis.

The total cost in terms of  $\Delta V$  will be the sum of the different velocity increments of the seven maneuvers, in reference to table 4.1:

$$\Delta V = \Delta V_1 + \Delta V_2 + \Delta V_3 + \Delta V_4 + \Delta V_5 + \Delta V_6 + \Delta V_7 \quad (4.1)$$

### 4.3.1 Capture and Escape

The first burn consists of the insertion into the first bi-elliptic parking orbit from the hyperbolic trajectory. To allow a wider range of solutions and optimize the cost of this first maneuver, the burn is non-tangential and not necessarily performed at periapsis, but in its proximity. This method has been used as presented by Cornick and Seversike in 1970 [18]. The first elliptic transfer orbit B is defined by its orbital parameters, four of which, true anomaly, inclination, argument of periapsis and longitude of the ascending node, as seen in table 4.3, are to be directly optimized, while the other two, semi-major axis and eccentricity, through the definition of the periapsis radius, are user defined. These four optimized parameters, are also necessary to evaluate the hyperbole A orbital parameters.

The unit vector towards the ascending node of orbit B is:

$$\hat{n}_B = L_{\Omega B} L_{iB} \hat{I} \quad (4.2)$$

where  $L_{\Omega B}$  and  $L_{iB}$  are rotation matrices, rotating the reference frame from the perifocal coordinate system to the Mars-centric equatorial one, together with  $L_{\omega B}$ . These are defined, in general, as:

$$L_{\Omega} = \begin{bmatrix} \cos \Omega & -\sin \Omega & 0 \\ \sin \Omega & \cos \Omega & 0 \\ 0 & 0 & 1 \end{bmatrix} \quad (4.3)$$

$$L_i = \begin{bmatrix} 1 & 0 & 0 \\ 0 & \cos i & -\sin i \\ 0 & \sin i & \cos i \end{bmatrix} \quad (4.4)$$

$$L_\omega = \begin{bmatrix} \cos \omega & -\sin \omega & 0 \\ \sin \omega & \cos \omega & 0 \\ 0 & 0 & 1 \end{bmatrix} \quad (4.5)$$

The true anomaly at capture, in orbit B perifocal frame, is:

$$\nu_{capt} = 2\pi + \rho_B - \omega_B \quad (4.6)$$

where  $\rho$  is the angle between the ascending node and the injection point in the transfer orbit B.

Knowing the true anomaly, it is possible to evaluate the radius magnitude, the unit vector and the position vector at the injection point.

$$r_{capt} = \frac{a_B(1 - e_B^2)}{1 + e_B \cos \nu_{capt}} \quad (4.7)$$

$$\hat{r}_{capt} = L_{\Omega B} L_{iB} L_{\rho B} \hat{I} \quad (4.8)$$

$$\vec{r} = r \hat{r} \quad (4.9)$$

where  $L_{\rho B}$  is a rotation matrix defined in general as:

$$L_\rho = \begin{bmatrix} \cos \rho & -\sin \rho & 0 \\ \sin \rho & \cos \rho & 0 \\ 0 & 0 & 1 \end{bmatrix} \quad (4.10)$$

The magnitude of the velocity after the capture burn of the orbit B can be determined from the energy conservation equation (3.19) as follows:

$$V_B = \sqrt{\frac{2\mu}{r} - \frac{\mu}{a_B}} \quad (4.11)$$

To compute the velocity unit vector, the unit vector  $\hat{I}$  must be rotated:

$$\hat{V}_B = L_{\Omega B} L_{iB} L_{\rho B} L_{\gamma B} \hat{I} \quad (4.12)$$

where  $L_{\gamma B}$  is the flight path angle  $\gamma$  rotation matrix. Said angle is defined as:

$$\gamma = \arcsin\left(\frac{\sqrt{\mu a_B(1 - e_B^2)}}{r V_B}\right) \quad (4.13)$$

with

- $0 \leq \gamma \leq \frac{\pi}{2}$  if  $0 \leq \nu \leq \pi$

- $\frac{\pi}{2} < \gamma < \pi$  if  $\pi < \nu < 2\pi$

$$L_\gamma = \begin{bmatrix} \cos \gamma & -\sin \gamma & 0 \\ \sin \gamma & \cos \gamma & 0 \\ 0 & 0 & 1 \end{bmatrix} \quad (4.14)$$

The velocity vector at injection point is:

$$\vec{V}_B = \hat{V}_B V_B \quad (4.15)$$

The velocity vector  $V_B$  and the radius vector  $r_B$  are necessary to evaluate the  $\Delta V$  and many orbital parameters of the orbit A.

The hyperbolic orbit A is defined by three parameters:

- $C_3$ : vis-viva energy integral
- $\alpha$ : right ascension of the hyperbolic asymptote
- $\delta$ : declination of the hyperbolic asymptote

These conditions depend on the Julian Date of the capture, and are predetermined.

The vis-viva energy is a function of the velocity at infinity, therefore at the limit of Mars sphere of influence. It can be expressed as:

$$C_3 = V_\infty^2 \quad (4.16)$$

The right ascension and the declination are necessary to pass from the hyperbolic reference frame the Mars reference frame, in which  $\hat{I}$ ,  $\hat{J}$  and  $\hat{K}$  are the three unit vectors along the X, Y and Z axis respectively. In particular, the unit vector in direction of the hyperbolic asymptote, in XYZ, is defined as:

$$\hat{S} = L_\alpha L_\delta^T \hat{I} \quad (4.17)$$

where  $L_\alpha$  and  $L_\delta$  are the rotation matrices to pass from the hyperbolic reference frame to the Mars reference frame. They can be expressed as:

$$L_\alpha = \begin{bmatrix} \cos \alpha & -\sin \alpha & 0 \\ \sin \alpha & \cos \alpha & 0 \\ 0 & 0 & 1 \end{bmatrix} \quad (4.18)$$

$$L_\delta^T = \begin{bmatrix} \cos \delta & 0 & \sin \delta \\ 0 & 1 & 0 \\ -\sin \delta & 0 & \cos \delta \end{bmatrix} \quad (4.19)$$

The semi-major axis of the hyperbola can be found from Mars gravitational parameter  $\mu$  and the vis-viva energy as:

$$\mu = 42828 \frac{km^3}{s^2} \quad (4.20)$$

$$a_h = \frac{\mu}{C_3} \quad (4.21)$$

Two hyperbolas are now possible with these conditions. In fact, the injection maneuver can be achieved on both the incoming and the outgoing leg of the hyperbola. This results into two possible values of the angle  $\beta$ , which is the angle between the injection position vector  $\vec{r}$  and the hyperbolic asymptote  $\hat{S}$ . A parallel analysis is carried out for both values of  $\beta$  and the one that guarantees a smaller value of  $\Delta V$  is chosen. It has been found after numerous computation that the optimal injection happens when the motion of the hyperbola is in the same direction as the motion of the transfer orbit B. The two angles  $\beta$  are defined as:

$$\beta_1 = \arccos(\vec{r} \cdot \hat{S}) \quad (4.22)$$

$$\beta_2 = 2\pi - \arccos(\vec{r} \cdot \hat{S}) \quad (4.23)$$

Knowing  $\beta$ , it is possible to evaluate  $\phi_a$ , namely the true anomaly of the hyperbolic asymptote in the hyperbola, and  $\phi$ , the true anomaly of the injection point in the hyperbola, as:

$$\tan(\phi_a) = \sigma \sin \beta + \sqrt{(1 + \sigma)^2 - (1 - \sigma \cos \beta)^2} \quad (4.24)$$

$$\phi = \phi_a - \beta \quad (4.25)$$

where  $\sigma$  is a dimensionless parameter defined as:

$$\sigma = \frac{C_3 r_{capt}}{2\mu} \quad (4.26)$$

The hyperbolic eccentricity can be computed from  $\phi_a$  as either of these formulas:

$$e_h = \sqrt{\tan^2(\phi_a) + 1} \quad (4.27)$$

$$e_h = -\frac{1}{\cos \phi_a} \quad (4.28)$$

The radius of the injection point can now also be evaluated in terms of the hyperbolic parameters as:

$$r = \frac{a_h(e_h^2 - 1)}{1 + e_h \cos \phi} \quad (4.29)$$

Before the evaluation of the hyperbolic velocity vector, it is still necessary to find the hyperbolic flight path angle  $\gamma_h$ , which depends on the hyperbolic velocity magnitude  $V_h$  and the hyperbolic specific angular momentum magnitude  $h_h$ , and the unit vector direction of the hyperbolic specific angular momentum  $\vec{w}_h$ . These quantities have expression:

$$V_h = \sqrt{C_3 + \frac{2\mu}{r_{capt}}} \quad (4.30)$$

$$h_h = \sqrt{a_h \mu (e_h^2 - 1)} = \mu \sqrt{\frac{e_h^2 - 1}{C_3}} \quad (4.31)$$

$$\hat{w}_h = \frac{\hat{r}_{capt} \times \hat{S}}{\sin \beta} \quad (4.32)$$

The expression for  $\gamma_h$  is:

$$\gamma_h = \arcsin \frac{h_h}{r_{capt} V_h} \quad (4.33)$$

with:

- $0 \leq \gamma_h \leq \frac{\pi}{2}$  for  $0 \leq \phi \leq \pi$
- $\frac{\pi}{2} < \gamma_h < \pi$  for  $\pi < \phi < 2\pi$

The unit vector direction of the hyperbolic velocity is:

$$\hat{V}_h = \hat{r}_{capt} \cos \gamma_h + (\hat{w}_h \times \hat{r}_{capt}) \sin \gamma_h \quad (4.34)$$

Therefore, the hyperbolic velocity vector at the injection point is:

$$\vec{V}_h = V_h \hat{V}_h \quad (4.35)$$

It is finally possible to compute the velocity increment  $\Delta V$  vector of the first orbital maneuver:

$$\Delta \vec{V}_1 = \vec{V}_B - \vec{V}_h \quad (4.36)$$

The escape parameters use the same equations, only referring to the orbit I instead of orbit B for the bi-elliptical orbit related values. The only difference lays in the computation of the angle  $\phi_a$ , that for the escape maneuver has expression:

$$\tan \phi_a = -\sigma \sin \beta - \sqrt{(1 + \sigma)^2 - (1 - \sigma \cos \beta)^2} \quad (4.37)$$

### 4.3.2 Plane change at apoapsis

There are three maneuvers of plane change: burn 2, burn 4 and burn 6. Each of these is performed at apoapsis to reduce the  $\Delta V$  request and twist the orbital plane around the line of apsides. This type of maneuver requires an out of orbit plane burn, that will modify the inclination  $i$ , the longitude of the ascending node  $\Omega$  and, in case of elliptical orbits, also the argument of periapsis  $\omega$ , while leaving the semi-major axis  $a$ , the eccentricity  $e$  and the true anomaly  $\nu$  unchanged [16]. It is a very expensive maneuver, as it goes to vary only the direction of velocity, without changing the orbit energy, as the semi-major axis remains constant. In general, the magnitude of the velocity variation is:

$$\Delta V = 2v_\theta \sin \frac{\Delta\psi}{2} = 2\left[\frac{\mu}{h}(1 + e \cos \nu)\right] \sin \frac{\Delta\psi}{2} \quad (4.38)$$

where  $v_\theta$  is the tangential velocity, equal to the velocity at apoapsis, and  $\psi$  is the heading angle, namely the angle between the north direction and the velocity direction. The heading angle can be expressed as:

$$\psi = \arcsin \frac{\cos i}{\cos \delta} \quad (4.39)$$

where  $\delta$  is the declination of the point where the maneuver takes place, in this case the apoapsis, and is evaluated from the knowledge of the position vector in XYZ reference frame as (3.29):

$$\delta = \arcsin \frac{r_Z}{r}$$

The velocity direction after the burn is computed rotating the previous velocity of  $\Delta\psi$  around the apoapsis direction, that doesn't change, as the maneuver is carried out at apoapsis. Also, since the maneuver is operated at apoapsis, the angle between the velocity before the burn and after is  $\Delta\psi$ . Thus, knowing  $\vec{V}$  after the burn, it is possible to find the specific angular momentum  $\vec{h}$  (3.6), the node vector  $\hat{n}$  (3.32) and the eccentricity vector  $\vec{e}$  (3.16) and from these both  $\Omega$  (3.35) and  $\omega$  (3.36).

### 4.3.3 Apoapsis height variation

The apoapsis height variation is an in-plane tangential orbit transfer that occurs at periapsis. There are two maneuvers of this type: burn 3 and burn 5. The first one lowers the height of apoapsis from the bi-elliptic orbit one to the one of the parking orbit, while the second, burn 5, raises the height of the parking orbit apoapsis back into the one of the bi-elliptic orbit, to prepare for the escape maneuver. In this case, there are no optimized parameters, as the semi-major axis of both orbits are defined and the height of the periapsis does not vary. The only other orbital parameter to change, apart from  $a$  is the eccentricity  $e$ .

The magnitude of the velocity variation has expression:

$$\Delta V = \sqrt{-\frac{\mu}{a_2} + \frac{\mu}{a_1} + V_{1,p}^2} - V_{1,p} \quad (4.40)$$

where  $a_1$  and  $a_2$  are respectively the semi-major axis before and after the maneuver, and  $V_{1,p}$  is the velocity at periapsis before the burn. The latter has the following expression, derived from (3.19):

$$V_{1,p} = \sqrt{-\frac{\mu}{a_1} + \frac{2\mu}{r}} \quad (4.41)$$

The eccentricity after the burn is found from the expression (3.13) as:

$$e_2 = -\frac{r_{2,p}}{a_2} + 1 \quad (4.42)$$

### 4.3.4 Perturbations propagation

Mars oblateness causes secular perturbations on the parking orbits longitude of the ascending node and on their argument of periapsis. Since the stay time of a round-trip mission to Mars is fairly long, these orbital elements variation have to be taken into consideration. They depend on the size of the orbit, its inclination, its shape and the  $J_2$  harmonic coefficient, that describes the mass and physical properties of Mars, through the coefficients  $K_2$  and  $K_4$ . The variation velocity have the expression:

$$\dot{\Omega} = -\tau \cos i \left[ 3 \frac{K_2}{p^2} + 10 \frac{K_2}{p^4} (1 + 1.5e^2)(1 - 1.75 \sin^2 i) \right] \quad (4.43)$$

$$\dot{\omega} = \tau \left[ 3 \frac{K_2}{p^2} (1 - 1.5 \sin^2 i) + 10 \left( \frac{K_2}{p^4} \right) (1 + 0.75e^2)(1 - 5 \sin^2 i + 4.375 \sin^2 i) \right] + \dot{\Omega} \cos i \quad (4.44)$$

where:

$$\tau = \sqrt{\frac{\mu}{a^3}} \quad (4.45)$$

$$K_2 = \frac{7.03656 * 10^5}{\tau^2} \quad (4.46)$$

$$K_4 = \frac{2.2517 * 10^6}{\tau^2} \quad (4.47)$$

$\tau$  is also known as the mean motion of the orbit, as it describes the angular velocity of the spacecraft during the orbit.

Therefore, the variation of the two orbital elements influenced by Mars oblateness is:

$$\Delta\Omega = \dot{\Omega}t_{prop} \quad (4.48)$$

$$\Delta\omega = \dot{\omega}t_{prop} \quad (4.49)$$

where the time of propagation  $t_{prop}$  is expressed in days.

## 4.4 MATLAB implementation

The MATLAB genetic algorithm functions are detailed in section 2.9. To implement the optimization of the bi-elliptic apotwist maneuvers, eight parameters have been optimized (table 4.3). They appear in the code in this order:

1.  $\omega_B$  [rad], the argument of periapsis of the first bi-elliptic transfer orbit B.
2.  $\Omega_B$  [rad], the longitude of the ascending node of the first bi-elliptic transfer orbit B.
3.  $\rho_{capt}$  [rad], the angle between the ascending node and the capture injection point in the bi-elliptic orbit B. Equivalently, the true anomaly of the capture burn  $\nu_{capt}$  could have been used, as the two parameters depends on each other through the expression (4.6).
4.  $\rho_{esc}$  [rad], the angle between the ascending node and the escape ejection point to the hyperbolic orbit. In the same as way the previous parameter, this can be substituted with the true anomaly of the escape burn  $\nu_{esc}$ .
5.  $i_B$  [rad], the inclination of the first bi-elliptic transfer orbit B.

6.  $t_{DE}$  [days], the portion of the stay time in which the parking orbit D precesses into the orbit E.
7.  $i_F$  [rad], the inclination of the parking orbit F after the apotwist, the second plane change.
8.  $i_I$  [rad], the inclination of the bi-elliptic transfer orbit I after the last plane change

The input parameters (table 4.2) are defined as global variables in MATLAB. This allows these variables to be available in every work space and eliminates the need to define the input variables inside the optimization function. The options and the algorithm call have been coded as follows:

```

1 options = optimoptions('ga','SelectionFcn',@selectionstochunif,...
2     'EliteCount',10,...
3     'CrossoverFraction',0.2,...
4     'FunctionTolerance',1e-7,...
5     'PopulationSize',250,...
6     'PlotFcn',{'@gaplotbestf','@gaplotmaxconstr'},...
7     'Display','iter',...
8     'InitialPopulationRange',[0;t_stay],...
9     'MigrationDirection','both');
10
11 [optimal_parameters,DV_TOTAL,val,output,population,scores]=ga(
    @optim_7burns,8,[],[],[],[],LB,UB,[],options);

```

where the options functions are the syntax of the 'ga' call have already been explained in section 2.9. The other parameters are:

- DV\_TOTAL is the total  $\Delta V$  of the 7 burns, the function of be optimized.
- @optim\_7burns is the objective function, which describes the analytical computation of the total  $\Delta V$ .
- LB is the lower bound of the optimized parameters. In particular, in this case, referring to the order in which the variables are called,  $LB=[0\ 0\ 0\ 0\ 0\ 0\ 0]$ .
- UB defines the upper bound of the optimized parameters. In this optimization, this element has the form of  $UB=[2\pi\ 2\pi\ 2\pi\ 2\pi\ \pi\ \pi\ t_{stay}\ \pi]$

## 4.5 Results

After the development of the code that computes the optimal solution using genetic algorithms, this has been used to optimize the characteristics of the parking orbits of three missions, and, doing so, to verify the algorithm solutions quality.

In particular, the data of three different orbital missions in 2037, 2041 and 2045, have been taken into consideration, as presented in "Optimizing Parking Orbits for Roundtrip Mars Missions" [17]. These data describe the hyperbolic orbits of arrival and departure from Mars and the stay time on the planet of each mission for spacecrafts using chemical propulsion, and are presented in table 4.4.

**Table 4.4:** Hyperbolic trajectories data[17]

Mission Launch Year	2037	2041	2045
$C_{3capt}$ [ $\frac{km^2}{s^2}$ ]	7.7785	8.5264	11.1155
$\alpha_{capt}$ [ $deg$ ]	19.4	113.8	162.9
$\delta_{capt}$ [ $deg$ ]	38.7	-1.7	-34.0
$C_{3esc}$ [ $\frac{km^2}{s^2}$ ]	9.5914	6.1058	7.6010
$\alpha_{esc}$ [ $deg$ ]	-124.1	-53.5	34.3
$\delta_{esc}$ [ $deg$ ]	8.7	5.3	31.6
$t_{stay}$ [ $days$ ]	352.8	368.7	480

#### 4.5.1 Orbital missions comparison

Orbital missions do not present particular constraints, as the spacecraft is assumed to orbit around the planet for the entire stay time. The requirements are therefore connected with which parking orbit may be functional to the mission. For this study, the periapsis, which, as shown in section 4.2, is one of the input parameters, is assumed to be of 250 km of altitude. The semi-major axis of the bi-elliptic transfer orbits is assumed to be equivalent of an orbit of 10-sol period, while the semi-major axis of the parking orbit is assumed to be equivalent of an orbit of 1-sol period. Sol is the name to the Martian day, which is approximately 24 hours, 39 minutes and 35 seconds long. Mars mean radius is 3389.5 km. Therefore, the values required as input to the code will be:

- $r_P = 3639.5 \text{ km}$
- $a_{bi-el} = 94911 \text{ km}$
- $a_{PO} = 20448 \text{ km}$

The last parameter to define is the inclination of the desired parking orbit. This has been chosen of  $170^\circ$  for all the three missions.

The code has been run numerous times to unsure a solution as close to the optimal one as possible, and results of this analysis are reported on table 4.5.

**Table 4.5:**  $\Delta V$  of the three different missions

		<b>2037</b>	<b>2041</b>	<b>2045</b>
$\Delta V_1$	$\frac{km}{s}$	0.8168	0.8578	1.1001
$\Delta V_2$	$\frac{km}{s}$	0.0553	0.0023	0.0417
$\Delta V_3$	$\frac{km}{s}$	0.1742	0.1742	0.1742
$\Delta V_4$	$\frac{km}{s}$	0.0257	0.0031	0.0028
$\Delta V_5$	$\frac{km}{s}$	0.1742	0.1742	0.1742
$\Delta V_6$	$\frac{km}{s}$	0.0027	0	0
$\Delta V_7$	$\frac{km}{s}$	0.9528	0.6399	0.7827
$\Delta V_{TOT}$	$\frac{km}{s}$	2.2015	1.8514	2.2757

From the data it is clear that the capture and escape burns costs increase with a higher vis-viva energy of the hyperbolic trajectories. This comes to no surprise, as this energy is square of the hyperbolic excess speed  $V_\infty$ . A higher  $V_\infty$  will necessarily mean a higher velocity before the capture burn, or after the escape one, leading to a higher velocity increment. Of course, the third and fifth burns have equal cost for every mission, as the apoapsis height change maneuver is not affected by the optimization.

### Two burns method comparison

To validate how convenient the bi-elliptic technique is, it has been compared to a two burns method. In this case, only two maneuvers take place: the capture and escape burns. These are still computed as non-coplanar, non-tangential and off periapsis. The capture burn will directly insert the spacecraft from the arrival hyperbolic orbit into an orbit of the required inclination (which will still be  $170^\circ$  to compare the data with the ones listed in table 4.5) of either 1-sol period or 10-sol period, then the orbit will precess for the entire stay time according to the same perturbation model detailed in 4.3.4. From the precessed orbit, the spacecraft performs the escape burn into the return hyperbolic trajectory.

The results of the 2 burns approach are displayed in table 4.6.

These data show how the bi-elliptic apotwist maneuver is a less expensive way to reach the desired 1-sol parking orbit in every mission considered. The saving in terms of total velocity increment, though, varies greatly among the missions. In particular, the 2041 mission data display a much smaller difference between the two approaches. This could be due to the fact that the conditions of this mission are peculiarly favorable. In fact, the stay time can naturally allow the arrival parking orbit to precess into an optimal, or close to optimal, departure parking orbit.

**Table 4.6:** 2 burns technique comparison

Launch Year			2037	2041	2045
$\Delta V_{TOT}$	$\frac{km}{s}$	<b>7 burns</b>	2.2015	1.8514	2.2757
$\Delta V_{TOT}$	$\frac{km}{s}$	<b>2 burns, 1-sol</b>	3.3858	1.9655	4.3014
$\Delta V_{TOT}$	$\frac{km}{s}$	<b>2 burns, 10-sol</b>	2.6772	1.5653	3.7798

Furthermore, the inclination of the parking orbit is possibly advantageous, too, making the plane changes less decisive. The geometry of the hyperbolic trajectories of arrival and departure, in fact, determines the plane in which these orbits lay. If the parking orbit does not require severe plane changes, as its inclination is already close to the ones of the hyperbolic trajectories of capture and departure, the saving in terms of  $\Delta V$  of the bi-elliptic apotwist method will be lower. On the contrary, if the plane change to reach the parking orbit is substantial, eliminating the plane change maneuvers at apoapsis will increase significantly the reorientation cost, making the 2-burn technique total  $\Delta V$  much higher than the one of the bi-elliptic apotwist method. In fact, the 2-burn method needs to achieve the changes of inclination from the arrival hyperbolic trajectory to the parking orbit only in the capture maneuver, which is performed close to the orbit periapsis, where the spacecraft velocity is high, increasing the maneuver cost, compared to a plane change at apoapsis as in the bi-elliptic apotwist method. In the same way, the second and third plane changes in the bi-elliptic method, performed at apoapsis, allow the spacecraft to reorient optimally for the escape maneuver.

The 2 burns technique applied to reach a 10-sol parking orbit has a lower cost compared to the same method used to reach 1-sol. The saving in terms of  $\Delta V$  is significant, but it does not come as surprising, as the velocity near periapsis of such orbit is higher, therefore closer to the velocity of the hyperbolic trajectory, making the necessary velocity increment lower. The total cost is still significantly higher than the bi-elliptic apotwist method, with parking orbit at 1-sol, for the 2037 and the 2045 missions, while it is lower for the 2041 mission.

### Apoapsis height

To verify the impact of the semi-major axis of the parking orbit  $a_{PO}$  on the total cost of the mission in terms of  $\Delta V$ , maintaining constant the periapsis radius, the semi-major axis has therefore been raised to be equivalent to an orbit of 2-sol period. As the burns to modify the height cost are constant through every mission, the behavior should be similar for all three missions.

The value of the 2-sol semi-major axis and the value of the apoapsis height change maneuver are:

- $a_{PO} = 32459 \text{ km}$
- $\Delta V_{3-5} = 0.0912 \frac{\text{km}}{\text{s}}$

The results are listed in table 4.7.

**Table 4.7:** Influence of the variation of  $a_{PO}$  on  $\Delta V$

Launch Year			2037	2041	2045
$\Delta V_{TOT}$	$\frac{\text{km}}{\text{s}}$	<b>1-sol</b>	2.2015	1.8514	2.2757
$\Delta V_{TOT}$	$\frac{\text{km}}{\text{s}}$	<b>2-sol</b>	2.0558	1.7183	2.1050

The results confirm the logical prediction: the total cost of the maneuvers is lower for every mission than the equivalent mission with the 1-sol period parking orbit. In fact, as the apoapsis height has increased, the maneuver to modify the second bi-elliptic transfer orbit of 10-sol period into the parking orbit of 2-sol period has significantly decreased from the 1-sol case. Furthermore, the apotwist maneuver, that takes place at apoapsis, will be less expensive too, as the magnitude of the apoapsis velocity has decreased.

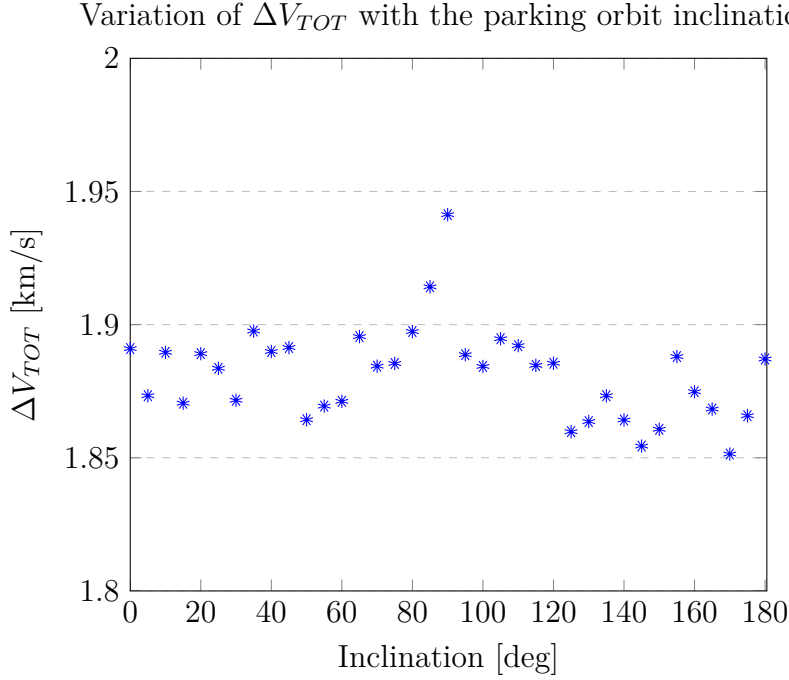
Despite the significant saving in terms of total  $\Delta V$ , a parking orbit of 2-sol period may not be apt for a surface mission of sample and return or of human exploration. In fact, the higher semi-major axis will increase the cost for descent and ascent maneuvers, as the velocity at periapsis will increase with it too.

### 4.5.2 The 2041 mission analysis

Considering only the 2041 mission, two more analysis have been carried out: the variation of the total  $\Delta V$  with the choice of the parking orbit inclination and a mass analysis, using data borrowed from preliminary studies of a manned Mars mission architecture.

#### Inclination

To study the influence of the inclination of the parking orbit D on the cost of the mission, the genetic algorithm has been run for every different inclination and the best solution has been chosen. The inclination has been varied with a  $5^\circ$  step, while the other parameters have been kept constant. The results are presented in the following chart.



All the  $\Delta V$  for the different inclinations are found in a range of approximately 100 m/s, with the polar orbit being the most expensive. The results do not highlight a definite trend, suggesting that the inclination does not impact significantly the overall cost of the mission, in terms of velocity increment. The variation among the results is most likely to be a product of the variability of solutions of the genetic algorithm approach. In fact, the presence of eight parameters to optimize has the consequence of the existence of many local optima, that the algorithm may find before the global optimal solution. The plane change maneuvers carried out at apoapsis, where, due to the low velocity of the spacecraft, the cost of this type of burn is limited, allow to reach parking orbits of every inclination with a similar cost.

## Mass

To carry out the mass analysis, it is firstly necessary to introduce how the masses at different phases of the mission have been computed. The basis of the mass computation is the Rocket Equation, or Tsiolkovsky Equation:

$$\Delta V = c \ln \frac{m_i}{m_f} \quad (4.50)$$

where  $c$  is the effective exhaust velocity, characteristic of the propulsion choice,  $m_i$  is the initial mass, before the burn, and  $m_f$  is the final mass, after the burn.

It is possible to find the expression of the final mass, inverting the previous equation, as:

$$m_f = m_i e^{\frac{\Delta V}{c}} \quad (4.51)$$

The propellant mass, which is the difference between the initial mass and the final mass, will thus has the following expression:

$$m_p = m_f - m_i = m_i \left[ 1 - e^{\frac{\Delta V}{c}} \right] \quad (4.52)$$

The value of  $c$  is obtained from the specific impulse, which is a known characteristic of the propulsion system, through the expression:

$$I_{sp} = \frac{c}{g_0} \quad (4.53)$$

where  $g_0 = 9,80665 \frac{m}{s^2}$  is the gravity acceleration on Earth at sea level.

To conduct the mass analysis, on the 2041 mission, the mass of the different elements of the spacecraft has been borrowed from a study of possible architectures for manned mission, conducted by NASA in 2015 [19]. In particular, the paper presents a solution for a hypothetical 2039 mission, which has similar characteristics, in terms of hyperbolic trajectories energy and stay time, with the mission that has been considered for the genetic bi-elliptic optimization.

This mission, that takes place in 2039, aim to the human exploration of Mars surface. Five landers are already pre-deployed and orbiting Mars before the arrival of the crew module. The Mars Ascent Vehicle, to bring the crew back into orbit, is also obviously pre-deployed. The crew module departs from Earth in 2039, using two Methane Cryogenic Propulsion Systems (MCPS), for Trans-Mars Injection (TMI) and Mars Orbit Injection (MOI), the Habitat Module and the Earth Orbit Injection (EOI) MCPS, which is not pre-deployed due to the low energy of the escape hyperbolic trajectory from Mars. To add to these elements, there is of course the propellant mass. The TEI (Trans-Earth Injection) stage is also pre-deployed.

Approaching Mars orbit, the spacecraft will consist of the MOI stage, the Habitat Module with the crew, the EOI stage and the total propellant for the following maneuvers. The propulsion system will then perform the capture maneuver and first reorientation maneuvers to insert into a 1-sol orbit. The crew stack then docks with a lander and the TEI stage. The crew enters the lander and departs for Mars surface, where they will operate for 300 days, before ascending into orbit again and return to Earth. At the departure from Mars, the spacecraft will consist of the Habitat Module, the TEI MCPS and the EOI MCPS. The total stay time on Mars surface and on Mars orbit is of 329 days.

The mass estimation of the previously described elements is listed in table 4.8. The mass of the EOI MCPS stage is wet, as this thesis does not evaluate burns to return into Earth orbit.

**Table 4.8:** Mass data[19]

	Mass [ton]
Habitat cabin	41.3
Single MCPS stage (dry)	7.5
EOI MCPS stage (wet)	18.3

The MCPS design and characteristics are depicted in figure 4.2. The specific impulse has been used in the following computations.

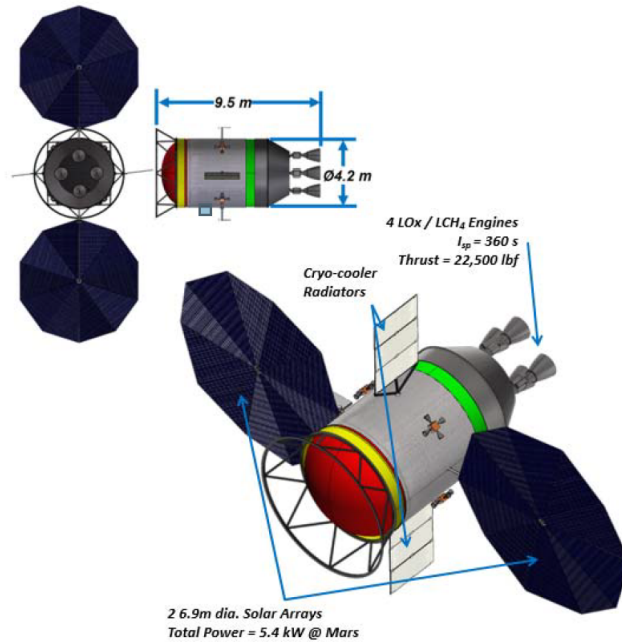


**Figure 4.2:** MCPS design [19]

Using the results summarized in table 4.5 for the 2041 mission, assuming the propulsion system to be the MCPS, the masses to be as described in table 4.8 and the propellant to have a 12 % margin for safety, it has been found that the total initial mass, at Mars arrival, is equal to approximately 120 ton. The initial and final masses, together with the necessary propellant masses, for every maneuver are listed in table 4.9.

**Table 4.9:** Mass analysis results

	$\Delta V$ $\frac{km}{s}$	Initial mass[kg]	Final Mass[kg]	Propellant Mass[kg]
$\Delta V_1$	0.8578	119988.02	91739.31	28248.71
$\Delta V_2$	0.0023	91739.31	91672.43	66.88
$\Delta V_3$	0.1742	91672.43	86759.22	4913.21
$\Delta V_4$	0.0031	86759.22	86673.97	85.25
$\Delta V_5$	0.1742	86673.97	82028.65	4645.3
$\Delta V_6$	0	82028.65	82028.65	0
$\Delta V_7$	0.6399	82028.65	67100	14928.65

# Chapter 5

## Conclusions

This master thesis has presented the analytical development of the bi-elliptic apotwist parking orbits selection technique for a roundtrip mission to Mars and the implementation of a genetic algorithm in MATLAB to optimize the overall  $\Delta V$  cost during the stay in Mars sphere of influence. The bi-elliptic apotwist method, introduced by Qu, Merrill, Chai and Kosar, consists of seven maneuvers that capture the spacecraft from its interplanetary trajectory into a target parking orbit and then reorient it to escape Mars gravity well.

Genetic algorithms, based on the principles of Darwinian genetics, have been successfully implemented for the optimization of the parking orbit reorientation. These type of optimization algorithms always converge to a solution of the given problem, they are apt to work with numerous variables, as in this case, and their computational times are limited.

The MATLAB genetic code created to implement the bi-elliptic apotwist maneuvers has been run to evaluate the reorientation method effectiveness, using as input parameters some pre-existing data of hyperbolic trajectories of arrival and departure from Mars, referred to three different missions. The analysis has shown how this method can substantially lower the velocity increment request to reorient the spacecraft in comparison with a simpler two-burn technique. The magnitude of this saving in total cost differs among the three missions considered, as the geometry of the hyperbolic trajectories influences the impact of the three plane change maneuvers of the bi-elliptic apotwist method. In fact, if the inclinations of the interplanetary orbits are close to the inclination of the parking orbit, changing the orbital plane during the capture and escape burns only, as in the 2-burn method, does not greatly increase the overall cost. Furthermore, it has been studied how the total  $\Delta V$  of the reorientation maneuvers changes with the variation of two parameters: the inclination and the semi-major axis of the parking orbit. While the first analysis showed that the inclination does not considerably affect the mission cost, the choice of a higher semi-major axis significantly decreases the  $\Delta V$  request.

A higher semi-major axis, despite lowering the reorientation cost, negatively impacts the cost of the descent and ascent maneuvers for a surface mission. Finally, using the optimized  $\Delta V$  for the 2041 mission and data of the preliminary mission architecture for a hypothetical manned mission to Mars, a mass estimation has been carried out, showing that the mass of the spacecraft entering Mars sphere of influence is approximately of 120 ton.

Future studies should analyze different types of missions in which the bi-elliptic apotwist can be applied and optimized via genetic algorithms; in particular, the exploration of Mars natural satellites, Phobos and Deimos. This will require different constraints and a N-body problem physical model, rather than the two-body problem approach utilized within this thesis' study. Also, considering a Mars surface mission, as in this thesis, it should be studied how to target a particular landing site and optimize the parking orbits that allow it. This would mean introducing new constraints, regarding for example the argument of periapsis of the parking orbit and its longitude of the ascending node, other than the already considered inclination. Moreover, the optimization should be developed for hybrid propulsion, other than the chemical propulsion one, thus modifying the analytical computation of the velocity increments to fit a non-impulsive maneuvers.

# Bibliography

- [1] N. S. Amade J. Wertz. «Design of a Mars Rapid Round Trip Mission». In: *AIAA SPACE 2010 Conference & Exposition*. DOI: 10.2514/6.2010-8642. eprint: <https://arc.aiaa.org/doi/pdf/10.2514/6.2010-8642>. URL: <https://arc.aiaa.org/doi/abs/10.2514/6.2010-8642> (cit. on p. 1).
- [2] A. Fraknoi D. Morrison S. C. Wo. *Astronomy*. Houston, Texas: OpenStax, 2018 (cit. on p. 1).
- [3] E. Siegel. «The 5 Possibilities For Life On Mars». In: *Forbes* (Aug. 2020) (cit. on p. 1).
- [4] European Space Agency. *Why go to Mars?* 2020. URL: [https://www.esa.int/Science\\_Exploration/Human\\_and\\_Robotic\\_Exploration/Exploration/Why\\_go\\_to\\_Mars](https://www.esa.int/Science_Exploration/Human_and_Robotic_Exploration/Exploration/Why_go_to_Mars) (cit. on p. 1).
- [5] Bret Drake, Stephen Hoffman, and David Beaty. «Human exploration of Mars, Design Reference Architecture 5.0». In: July 2009. DOI: 10.1109/AERO.2010.5446736 (cit. on pp. 2, 4).
- [6] R. G. Merrill D. R. Komar M. Qu P. R. Chai. «Optimizing Mars Sphere of Influence Maneuvers for NASA’s Evolvable Mars Campaign». In: 2016 (cit. on pp. 4, 36, 37).
- [7] O. Kramer. *Genetic Algorithm Essentials*. Cham, Switzerland: Springer International Publishing AG, 2017 (cit. on p. 6).
- [8] M. Mitchell. *An Introduction to Genetic Algorithms*. Cambridge, Massachusetts: The MIT Press, 1998 (cit. on p. 6).
- [9] T. Bäck. *Evolutionary Algorithms in Theory and Practice*. New York, New York: Oxford University Press, 1996 (cit. on p. 6).
- [10] P. Fleming A. J. Chipperfield. «The MATLAB genetic algorithm toolbox». In: Feb. 1995, pp. 10/1–10/4. DOI: 10.1049/ic:19950061 (cit. on p. 6).
- [11] H. A. Loáiciga O. Bozorg-Haddad M. Solgi. *Meta-Heuristic and Evolutionary Algorithms for Engineering Optimization*. Hoboken, New Jersey: John Wiley & Sons, Inc., 2017 (cit. on p. 7).

- [12] Mathworks. *Global Optimization Toolbox Documentation*. 2020. URL: [https://it.mathworks.com/help/gads/index.html?category=index&s\\_tid=CRUX\\_topnav](https://it.mathworks.com/help/gads/index.html?category=index&s_tid=CRUX_topnav) (cit. on p. 18).
- [13] Mathworks. *Genetic Algorithm Documentation*. 2020. URL: <https://it.mathworks.com/help/gads/genetic-algorithm.html> (cit. on p. 18).
- [14] Mathworks. *ga Documentation*. 2020. URL: <https://it.mathworks.com/help/gads/ga.html#d122e38653> (cit. on p. 18).
- [15] R. R. Bate D. D. Mueller J. E. White. *Fundamentals of Astrodynamics*. New York, New York: Dover Publications, Inc., 1971 (cit. on pp. 21, 25).
- [16] D. A. Vallado. *Fundamentals of Astrodynamics and Applications*. Hawthorne, California: Microcosm Press, 2013 (cit. on pp. 21, 26, 32, 44).
- [17] M. Qu R. G. Merrill P. R. Chai D. Komar. «Optimizing Parking Orbits for Roundtrip Mars Missions». In: 2017 (cit. on pp. 35, 48).
- [18] D. E. Cornick L. K. Seversike. «Optimum Parking Orbit Orientation for a Three-Dimensional Capture-Escape Mission». In: 1970 (cit. on pp. 36, 39).
- [19] T. K. Percy M. McGuire T. Polsgrove. «In-Space Transportation for NASA's Evolvable Mars Campaign». In: 2015 (cit. on pp. 53, 54).